1   **Repression of an activity-dependent autocrine insulin signal is required for sensory**

2   **neuron development in *C. elegans***

3   Lauren Bayer Horowitz[1], Julia P. Brandt[1], and Niels Ringstad[1]*

4

5   [1.] Skirball Institute of Biomolecular Medicine, Helen L. and Martin S. Kimmel Center for Biology

6   and Medicine, Department of Cell Biology, Neuroscience Institute, NYU School of Medicine, New

7   York, NY 10016

8

9   *correspondence: Niels.Ringstad@med.nyu.edu

10

11

12

13

14

15

16

17

18

19

20

21

22

23

Abstract

Nervous system development is instructed both by genetic programs and activity-dependent refinement of gene expression and connectivity. How these mechanisms are integrated remains poorly understood. Here, we report that the regulated release of insulin-like peptides (ILPs) during development of the *C. elegans* nervous system accomplishes such an integration. We find that the p38 MAP kinase PMK-3, which is required for the differentiation of chemosensory BAG neurons, functions by limiting expression of an autocrine ILP signal that represses a chemosensory-neuron fate. ILPs are released from BAGs in an activity-dependent manner during embryonic development, and regulate neurodifferentiation through a non-canonical insulin receptor signaling pathway. The differentiation of a specialized neuron-type is, therefore, coordinately regulated by a genetic program that controls ILP expression and by neural activity, which regulates ILP release. Autocrine signals of this kind may have general and conserved functions as integrators of deterministic genetic programs with activity-dependent mechanisms during neurodevelopment.

Introduction

The nervous system comprises many neuron-types, each endowed with a unique physiology, connectivity and molecular profile. Diversity in neuronal form and function is required for the assembly of neural circuits that support complex brain functions and behaviors. Understanding how this diversity is generated during development remains a major question in neuroscience. A remarkable feature of nervous system development is that genetically encoded developmental programs cooperate with neural activity dependent processes to promote the differentiation of specific neuron-types and instruct neuronal connectivity (Wamsley and Fishell

2

47 2017). How these two different mechanisms - one specified and the other activity-dependent -

48 are integrated during nervous system development remains poorly understood.

49   The *C. elegans* nervous system displays a wide range of neuronal diversity, and is a

50 powerful model to study neuronal differentiation (White et al. 1986; Hobert et al. 2016). The

51 mostly invariant cell lineage that generates the *C. elegans* nervous system (Sulston 1977;

52 Sulston 1983) suggests that neuronal differentiation in *C. elegans* is principally determined by

53 genetic programs intrinsic to the cell-lineage. Indeed, many studies have identified transcription

54 factors that act in specific sub-lineages to promote specific neural fates (Hobert 2016). However,

55 there are also important roles for neuronal activity during development of the *C. elegans* nervous

56 system. For example, there is a striking role for activity of embryonic AWC chemosensory

57 neurons in determining their differentiation into functionally distinct subtypes (Troemel 1999;

58 Sagasti 2001). More recently, it has been found that there is a critical period during which neural

59 activity instructs circuit assembly in the *C. elegans* motor system (Barbagallo et al. 2017). Post-

60 developmentally, neural and sensory activity is required for maintaining the proper morphology

61 of chemosensory neurons (Peckol 1999; Mukhopadhyay et al. 2008), and for expression of

62 chemosensory receptors and neuropeptides that define specific chemosensory neuron fates

63 (Peckol et al. 2001; Gruner et al. 2014; Rojo Romanos et al. 2017). Like the vertebrate nervous

64 system, therefore, development of the *C. elegans* nervous system requires both lineally

65 programmed gene regulation and neural activity.

66   We have investigated mechanisms required for the development of a pair of *C. elegans*

67 sensory neurons - the BAGs, which sense microbe-derived carbon dioxide (CO_2) to control

68 foraging behaviors (Brandt and Ringstad 2015). Properly specified BAG neurons are equipped

69 with a chemotransduction apparatus used to sense CO_2, which includes the receptor-type

3

70   guanylyl cyclase GCY-9 (Smith et al. 2013). They also express the neurotransmitter glutamate

71   (Serrano-Saiz et al. 2013) together with a specific set of neuropeptides *e.g.* the FMRF-amide

72   neuropeptides FLP-17, FLP-10 and FLP-19 (Kim and Li 2004). Previous studies identified a

73   number of transcription factors that promote the BAG neuron fate (Guillermin et al. 2011; Brandt

74   et al. 2012; Gramstrup Petersen and Pocock 2013; Rojo Romanos et al. 2015). However

75   mutants for these transcription factors still generate BAG neurons that differentiate to some

76   extent. Therefore, other mechanisms that promote a BAG fate must exist. Through a screen for

77   additional regulators of the BAG fate we identified the p38 MAP kinase (MAPK) PMK-3 (Brandt

78   and Ringstad 2015). PMK-3 is required during development, and post-developmental expression

79   of PMK-3 does not restore gene expression or function to *pmk-3* mutant BAG cells (Brandt and

80   Ringstad 2015). The phenotype of *pmk-3* mutants differs from that of transcription factor

81   mutants; *pmk-3* mutants are strongly defective in BAG-neuron function, but their gene-

82   expression defects are restricted to a subset of BAG-specific genes. Although it is clear that

83   PMK-3 functions in BAG development, how PMK-3 promotes differentiation of BAG neurons is

84   unknown. p38 MAPKs have many functions in the nervous system (Thomas and Huganir 2004),

85   but these functions are often part of injury- or stress-responses, and roles for p38 MAPKs in

86   neuronal differentiation remain poorly understood.

87   To determine how PMK-3 functions in BAG neuron development, we isolated and

88   characterized mutations that suppress the gene expression defects caused by loss of PMK-3.

89   Here we discover that a major complementation group of suppressor mutations comprises

90   alleles of *unc-31*, which encodes a factor required for the regulated secretion of neuropeptides

91   and hormones. Loss of *unc-31* restores gene expression to *pmk-3* mutant BAG cells by

92   interfering with the regulated release of insulin-like peptides (ILPs), which are overexpressed in

93   *pmk-3* mutants and repress expression of a BAG cell fate. These ILPs are released from BAG

94   neurons themselves and, therefore, function as an inhibitory autocrine signal during BAG neuron

95   development. This mechanism combines a gene regulatory program, to set levels of ILP

96   expression, and neural activity, which controls the release of ILPs during development, to

97   regulate the differentiation of a specific neuron-type. We propose that similar mechanisms might

98   function widely during nervous system development to integrate neural activity with genetically

99   specified developmental programs.

100

101   **Results**

102   ***pmk-3* mutant sensory neurons are defective in expression of a functionally important**

103   **neuropeptide and also have defects in sensory transduction and synapse formation.**

104   *pmk-3* mutants fail to express the BAG-neuron-specific FMRF-amide neuropeptide *flp-17*

105   (**Figure 1A**). FLP-17 peptides activate the $G_{i/o}$-coupled receptor EGL-6 to inhibit motor neurons

106   in the *C. elegans* egg laying system (Ringstad and Horvitz 2008), and were recently shown to

107   also be required for BAG-neuron-dependent CO_2 avoidance behavior (Guillermin et al. 2017;

108   Lee et al. 2017). To determine whether the behavioral defect of *pmk-3* mutants can be explained

109   by their failure to express *flp-17* neuropeptides, we compared the CO_2 avoidance defects of

110   *pmk-3* and *flp-17* mutants. Both *pmk-3* and *flp-17* mutants were severely defective for CO_2

111   avoidance, although *pmk-3* mutants displayed a more severe defect (**Figure 1B**). Interestingly,

112   we found that *egl-6* mutants, which lack the known receptor for FLP-17 peptide, were wild-type

113   for CO_2 avoidance (**Figure 1B**), suggesting that FLP-17 acts on distinct receptors in circuits that

114   mediate chemotaxis.

115   Because *pmk-3* mutants exhibited a stronger CO_2 avoidance defect than *flp-17* mutants,

116   we sought to determine whether PMK-3 regulates other aspects of BAG-neuron physiology or

117   structure. We first tested whether *pmk-3* mutant BAG cells exhibit sensory transduction defects

118   using *in vivo* calcium imaging to measure their calcium responses to CO_2 stimuli (Brandt et al.

119   2012). *pmk-3* mutant BAG cells responded to strong CO_2 stimuli, but their responses were

120   significantly smaller than those of the wild type (**Figure 1C-D, Figure S1**). When wild-type and

121   *pmk-3* mutant cell responses were scaled to unity, we observed no difference between the

122   dynamics of the calcium responses, indicating that the kinetics of cell activation was not altered

123   by *pmk-3* mutation (**Figure S1**).

124   We next tested whether *pmk-3* mutant BAG cells form proper synapses using GFP-

125   Reconstitution across Synaptic Partners (GRASP) (Feinberg et al. 2008) to label a subset of

126   BAG synapses. GRASP-puncta were observed throughout the axons of both wild type and

127   *pmk-3* mutant BAG cells (**Figure 1E**). We observed no significant difference in the number of

128   puncta in *pmk-3* mutants and in the wild type (**Figure S2**). The average size of puncta in *pmk-3*

129   mutants, however, was 18% smaller than that of the wild type (**Figure 1F**). From these data we

130   concluded that the behavioral defects of *pmk-3* mutants that are caused by their failure to

131   express FLP-17 neuropeptides are likely exacerbated by accompanying defects in BAG neuron

132   chemotransduction and synapse formation.

133

134   **Genes required for Ca^{2+}-dependent neural secretion suppress a neuropeptide gene**

135   **expression defect of *pmk-3* mutants.**

136   Previously, we found evidence that PMK-3 acts downstream of the Toll-like Receptor

137   TOL-1 to promote BAG neuron development (Brandt and Ringstad 2015). How PMK-3 itself

138   regulates expression of a BAG neuron fate was unknown. To address this question, we

139   performed a genetic screen for suppressors of the *flp-17* expression defects of *pmk-3* mutants.

140   From two screens that covered approximately 25,000 mutagenized haploid genomes, we

141   recovered 18 mutants in which BAG neuron expression of *flp-17* was restored to *pmk-3* mutants

142   (**Figure 2A-B**). Five of these mutants defined a major complementation group, and we decided

143   to further characterize the affected gene. These suppressor mutations strongly restored the

144   penetrance of *flp-17* reporter expression in *pmk-3* mutant BAG cells (**Figure 2C**), and also

145   significantly restored the levels of reporter expression (**Figure S3**). We asked whether the

146   suppressor mutations also affected another PMK-3 regulated gene. Expression of *gcy-33*, which

147   encodes a guanyly cyclase required for sensing hypoxia (Zimmer et al. 2009) and is regulated

148   by PMK-3 in BAG (Brandt and Ringstad 2015), was not restored in suppressed *pmk-3* mutants

149   (**Figure S4**). Therefore the suppressor gene defined by this complementation group has strong

150   effects on *flp-17* expression, but does not completely restore the *pmk-3* phenotype to wild-type.

151   Using high-resolution Single Nucleotide Polymorphism (SNP) mapping and whole-

152   genome sequencing we identified the suppressor gene as *unc-31* (**Figure 2D**), which encodes

153   the *C. elegans* homolog of Calcium-dependent Activator Protein for Secretion (CAPS).

154   UNC-31/CAPS is a neuron-specific factor required for docking and priming of dense core

155   vesicles (DCVs), which mediate the regulated release of neuropeptides, hormones and growth

156   factors (Speese et al. 2007; Zhou et al. 2007). Because of the known function of *unc-31*, we

157   hypothesized that Ca^{2+}-dependent secretion plays a role in BAG neuron development. We

158   tested whether mutations that affect other critical factors for neural secretion (**Figure 2E**) also

159   suppress *pmk-3*. Mutation of either UNC-13 or UNC-18, which like UNC-31 are required for

160   docking and priming of synaptic and dense core vesicles (Richmond 1999; Weimer et al. 2003),

161   strongly restored the frequency of *flp-17* expression to *pmk-3* mutants (**Figure 2F**). We also

162   tested a partial loss-of-function allele of the syntaxin homolog, UNC-64 (Saifee 1998), and

163   observed partial restoration of *flp-17* expression to *pmk-3* mutant BAG neurons (**Figure 2F**).

164   Because DCV exocytosis is triggered by elevated Ca^{2+} that enters cells through voltage-

165   gated calcium channels (VGCCs), we next tested whether mutation of VGCC subunits

166   suppresses the gene expression defect of *pmk-3* mutants. Mutation of the L-type VGCC alpha-1

167   subunit, *egl-19* (Lee 1997), did not restore *flp-17* expression to *pmk-3* mutants (**Figure 2G**). By

168   contrast, mutations in the NPQ-type VGCC alpha-1 subunit, *unc-2* (Schafer 1995), did suppress

169   *pmk-3* and significantly restored *flp-17* expression (**Figure 2G, Figure S5B**). The VGCC alpha-

170   2-delta subunit UNC-36 is a part of both L- and NPQ-type channels (Lee 1997). Partial loss of

171   UNC-36 function did not affect the frequency with which *pmk-3* mutants expressed *flp-17* but did

172   cause an increase in the expression levels of *flp-17* when it was expressed in *pmk-3* mutants

173   (**Figure S5**). Together, these data show that Ca^{2+}-dependent secretion and neural activity

174   antagonize PMK-3 dependent neuropeptide expression in BAG neurons.

175

176   **Neural activity during development regulates neuropeptide gene expression in BAG**

177   **neurons.**

178   *pmk*-3 functions cell-autonomously and during a critical period of embryonic development

179   to promote expression of *flp-17* in BAG neurons (Brandt and Ringstad 2015). We tested whether

180   neural activity and regulated secretion also act cell-autonomously in BAG neurons during the

181   same critical period. To dampen BAG activity, we used the BAG-neuron-specific and PMK-3-

182   independent *gcy-9* promoter (Smith et al. 2013; Brandt and Ringstad 2015) to overexpress the

183   inward rectifying potassium (K^+) channel IRK-1 (Emtage et al. 2012). IRK-1 expression in BAGs

8

184   restored *flp-17* expression to *pmk-3* mutants (**Figure 3A**). In parallel, we performed BAG-

185   targeted knockdown of *unc-31* using RNAi. Knock-down of *unc-31* in BAGs alone restored *flp-*

186   *17* expression to *pmk-3* mutant BAG neurons (**Figure 3B**). We compared the effects of BAG-

187   targeted IRK-1 expression or *unc-31* knock-down to the effects of disrupting neural activity and

188   regulated secretion in all neurons using a pan-neuronal promoter. BAG-targeted inhibition of

189   regulated secretion or neural activity suppressed *pmk-3* as strongly as the corresponding pan-

190   neuronal manipulations (**Figure 3A,B**). These data strongly suggest that neural activity and

191   UNC-31 function cell autonomously in BAGs to regulate *flp-17* expression.

192   We next tested when neural activity is required to exert its effect on *flp-17* expression.

193   We expressed *irk-1* under the control of a heat-shock-inducible promoter in *pmk-3* mutants.

194   Animals were heat-shocked as embryos, larvae, or adults to transiently induce *irk-1* expression

195   and reduce neural activity (**Figure 3C**), and were then scored for *flp-17* expression as adults.

196   The transgene for inducible expression of IRK-1 conferred some suppression in the absence of

197   heat shock, suggesting that it supports some basal expression of IRK-1 (**Figure 3D**). However,

198   heat-shock of embryos restored *flp-17* expression to *pmk-3* mutants above this baseline (**Figure**

199   **3D**). By contrast, induction of IRK-1 expression during larval or adult stages did not significantly

200   modify the *pmk-3* gene expression defect (**Figure 3D**). Together, these data indicate that, like

201   PMK-3, neural activity and UNC-31 are required during development in BAG neurons to regulate

202   neuropeptide gene expression.

203

204   ***pmk-3* mutation dysregulates expression of insulin-like genes in BAG neurons.**

205   Why might mutations in *unc-31* and other genes required for regulated secretion of

206   peptides suppress the effects of *pmk-3* mutation? We hypothesized that in *pmk-3* mutants a

9

207   factor, possibly a peptide hormone, is secreted by BAGs in an UNC-31-dependent manner and

208   inhibits their development. We sought evidence for such a secreted factor by transcriptionally

209   profiling embryonic BAG neurons from the wild type and *pmk-3* mutants. We used fluorescence-

210   activated cell-sorting to purify GFP-marked BAG neurons and 'non-BAG' non-fluorescent cells.

211   Differential gene expression analysis identified 692 transcripts whose expression significantly

212   differed between wild-type and *pmk-3* mutant BAG cells ($P < 0.05$) (**Figure 4A**). 189 of these

213   transcripts were also BAG-enriched, as determined by a comparison of wild-type BAG neurons

214   vs non-BAG cells ($P < 0.05$). Principal component analysis revealed that wild-type and *pmk-3*

215   mutant BAG cell transcriptomes are highly separable (**Figure 4B**), indicating that *pmk-3* is

216   required for proper expression of many genes in developing BAG neurons.

217   Inspection of genes affected by *pmk-3* mutation revealed that *pmk-3* mutant BAG cells

218   over-express multiple insulin-like peptides (ILPs) (**Figure 4C**). The ILP gene *daf-28*, which is

219   enriched in wild-type BAG neurons compared to non-BAG cells (**Figure S6**), is upregulated in

220   *pmk-3* mutant BAGs (**Figure 4D**). *ins-14, ins-29* and *ins-30*, which are not normally expressed

221   in wild-type BAGs, are clearly expressed in *pmk-3* mutant BAG neurons (**Figure 4E-G**). The

222   ILPs affected by *pmk-3* mutation all encode ILPs that are agonists of the *C. elegans* insulin/IGF-

223   like receptor (InR) DAF-2 (Kenyon 1993; Kimura 1997; Murphy and Hu 2013). Our RNA-Seq

224   data also revealed that an ILP gene that encodes an InR antagonist - *ins-1* (Cornils et al. 2011)

225   - is enriched in wild-type BAG neurons (**Figure S6**), but its expression is not affected by *pmk-3*

226   mutation (**Figure 4C**). These data suggested that defects caused by loss of PMK-3 might result

227   from excess expression of some ILPs expressed in embryonic BAGs. To test this hypothesis,

228   we next sought to determine how ILP production by BAGs regulates BAG neuron development.

229

An autocrine insulin signaling pathway antagonizes PMK-3 dependent gene expression in BAG cells.

To disrupt ILP production we used the dominant negative *daf-28(sa191)* allele (**Figure 5A**). *daf-28(sa191)* generates a non-functional ILP that mis-folds and disrupts production of other ILPs (Li et al. 2003). *daf-28(sa191)* phenocopied mutations that affect regulated secretion and restored *flp-17* expression to *pmk-3* mutants (**Figure 5B**). A deletion allele of *daf-28* (**Figure 5A**) also partially restored *flp-17* expression to *pmk-3* (**Figure 5C**), indicating that although BAGs produce several ILPS, DAF-28 has a non-redundant function in regulating BAG gene expression. We next overexpressed DAF-28(sa191) specifically in *pmk-3* mutant BAG neurons to test whether ILP production in BAG neurons themselves is required for their development. Overexpressing DAF-28(sa191) in BAGs strongly restored *flp-17* expression (**Figure 5B**). Together, these data indicate that ILP expression by BAGs antagonizes PMK-3-dependent expression of *flp-17*. Because *pmk-3* mutant BAGs overexpress ILPs, these data further suggest that the BAG neuron defects of *pmk-3* mutants are at least partly caused by dysregulated expression and release of ILPs.

ILPs released from BAGs might act on other cells that in turn release factors that regulate gene expression in BAGs. Alternatively, ILPs released from BAGs might function as autocrine signals and activate insulin-receptor signaling pathways in BAG themselves. To resolve these possibilities, we sought to determine the site of action of the InR signaling pathway that regulates *flp-17* expression in BAG neurons. First, we interrogated genes known to function in InR signaling for suppression of *pmk-3*. The InR DAF-2 signals via the phosphoinositide-3 (PI-3) kinase, AGE-1 (Morris 1996), and two serine/threonine kinases, AKT-1 and AKT-2 (Paradis 1998) (**Figure 5D**). Many genes that function in the canonical InR signaling pathway mutate to

11

253   suppress *pmk*-3; loss-of-function mutations in *daf-2*, *age-1*, and *akt-1*, each strongly restored

254   *flp-17* expression to *pmk-3* mutants (**Figure 5E**). We observed no effect, however, of *akt-2*

255   mutation on the *pmk-3* phenotype (**Figure 5E**). We next determined where the DAF-2 InR was

256   required for its role in the BAG neurons development. We tested the hypothesis that ILPs are

257   part of an autocrine signal, and performed BAG neuron-targeted knockdown of *daf-2* using RNAi.

258   Like the *daf-2* chromosomal mutation*,* BAG-targeted *daf-2* RNAi strongly restored *flp-17*

259   expression to *pmk-3* mutant BAG cells (**Figure 5F**). Together with our analysis of ILP expression

260   in BAGs, these data indicate that an autocrine ILP signal represses *flp-17* expression in BAG

261   neurons.

262

263   ***pmk-3* mutant BAG cells experience increased insulin signaling.**

264   InR-dependent phosphorylation inhibits entry of the Forkhead (FOXO) transcription factor

265   DAF-16 into the nucleus to regulate transcription (Lee 2001; Lin 2001). We used this

266   phenomenon to independently test the hypothesis that *pmk-3* mutation causes BAG neurons to

267   experience increased autocrine ILP signaling. We generated transgenic animals that express a

268   DAF-16::GFP fusion in BAG neurons, and we measured the ratio of nuclear DAF-16 to

269   cytoplasmic DAF-16 as an index of InR signaling in BAGs. This ratio varied among wild-type

270   BAG neurons, some of which showed little nuclear DAF-16::GFP fluorescence and others with

271   nuclear fluorescence that was comparable to that in the cytoplasm (**Figure 6A, left, middle**).

272   While *pmk-3* mutant BAG neurons also displayed a range of nuclear-to-cytoplasmic DAF-

273   16::GFP ratios, their distribution was significantly shifted towards lower ratios compared to those

274   measured in the wild type (**Figure 6B**), and on average had more cytoplasmic DAF-16::GFP. As

275   expected, mutation of the InR DAF-2 caused a dramatic accumulation of DAF-16::GFP in the

276   nuclei of BAG neurons (**Figure 6A, right**), but in *daf-2* mutants there was no significant effect of

277   *pmk-3* mutation on the ratios of nuclear to cytoplasmic DAF-16::GFP (**Figure 6C**). These data

278   indicate that *pmk-3* mutant BAG neurons experience elevated insulin signaling, and provide

279   independent corroboration of a model in which PMK-3 negatively regulates ILP expression and

280   InR signaling.

281

282   **InR/DAF-2 regulates neuropeptide expression independent of FOXO/DAF-16 in BAG**

283   **chemosensory neurons.**

284   We next tested whether the DAF-16/FOXO transcription factor, which is a canonical

285   effector of InR signaling, is required for ILPs to regulate *flp-17* expression. Because the *daf-16*

286   locus is tightly linked to the *flp-17* reporter that we use to assay the *pmk-3* mutant phenotype,

287   we used CRISPR/Cas9 to generate a new *daf-16* deletion allele in a strain carrying the *flp-17*

288   reporter (**Figure S7**). We did not observe an effect of *daf-16* mutation on the frequency of

289   animals that express *flp-17*, but we did note that these mutants express *flp-17* at lower levels

290   compared to the wild-type (**Figure S7**). Notably, knock-down of *daf-2* by RNAi still restored

291   expression of *flp-17* to *pmk-3* mutant BAG cells in the absence of *daf-16* (**Figure 5F**), indicating

292   that DAF-2 regulates *flp-17* expression in the absence of DAF-16. Mutating another transcription

293   factor that functions in the DAF-2 signaling pathway – the Nrf-like transcription factor SKN-1

294   (Tullet et al. 2008) – did not affect the penetrance or levels of *flp-17* expression (**Figure S7**).

295   Together, these data indicate that DAF-2 regulates gene expression in BAG neurons through a

296   mechanism independent from its canonical effector DAF-16. Although we could not rule out a

297   role for SKN-1 in this pathway, the absence of any effect of *skn-1* mutation on *flp-17* expression

298   suggests that this factor does not function in BAG neuron development.

13

299

Attenuating autocrine insulin signaling restores function to *pmk-3* mutant BAG neurons.

Mutation of PMK-3 dysregulates expression of ILP genes in BAG neurons, but also affects expression of many other genes (**Figure 4A**). To what extent is BAG neuron function affected by increased production of ILPs? To address this question we tested whether disrupting autocrine insulin signaling in BAGs restores CO_2 avoidance behavior to *pmk-3* mutants, which overexpress ILPs. We again used the dominant negative DAF-28(sa191) variant to disrupt insulin production in BAG neurons of *pmk-3* mutants, this time testing for effects of knocking down ILP production on behavior. We found that the chromosomal *daf-28(sa191)* mutation significantly restored CO_2 avoidance behavior to *pmk-3* mutants (**Figure 7A**). Overexpressing DAF-28(sa191) in *pmk-3* mutant BAG cells also suppressed the CO_2 avoidance defect of *pmk-3* mutants (**Figure 7B**), indicating that ILP production by BAGs is required for the effects of *pmk-3* mutation on behavior. Next, we asked whether disrupting *daf-2* function in BAGs could also restore behavior to *pmk-3* mutants. BAG-neuron-specific *daf-2* RNAi did not affect CO_2 avoidance by wild-type worms (**Figure 7C**), but significantly restored CO_2 avoidance to *pmk-3* mutants (**Figure 7C**). Together these data show that the functional defects caused by loss of PMK-3, which are associated with widespread changes in gene regulation, can be rescued by targeting the ILP signaling pathway in BAG neurons.

317

Discussion

We have found that the p38 MAP kinase PMK-3 controls development of *C. elegans* chemosensory BAG neurons through an unexpected mechanism: the regulation of an activity-dependent autocrine insulin signal (**Figure 7D**). This insulin signal is regulated at the level of

14

322 gene transcription. *pmk-3* mutant sensory neurons overexpress transcripts encoding insulin-like

323 peptides (ILPs). As a consequence, their BAG cells experience elevated DAF-2/Insulin Receptor

324 (InR) signaling, which antagonizes expression of a neuropeptide gene essential for their

325 function. We further show that the neuronal defects caused by loss of PMK-3 and concomitant

326 increases in ILP production are abolished in mutants with defects in activity-dependent neuronal

327 secretion. The autocrine insulin signal that controls expression of a chemosensory neuronal fate

328 is, therefore, controlled both by a cell-intrinsic PMK-3-dependent genetic mechanism and by

329 neural activity, which controls secretion of ILPs. This mechanism neatly integrates neural activity

330 with a developmental program of gene expression to regulate a neuronal cell fate.

331 Remarkably, although ILP genes represent only a fraction of the genes that are

332 dysregulated by loss of PMK-3 we found that it is possible to restore BAG-neuron function to

333 *pmk-3* mutants by only manipulating insulin signaling in BAG cells. Because of the central role

334 for ILP signaling in the etiology of the *pmk-3* mutant phenotype and because this mechanism

335 converges on regulation of genes with defined roles in neuron-function, it will be of great interest

336 to understand molecular mechanisms by which PMK-3 regulates ILP expression and how DAF-

337 2/InR signaling regulates expression of FLP-17 neuropeptides.

338

339 **Activity-dependent autocrine growth-factor signaling in the nervous system**

340 A key feature of ILP signaling in BAG neuron development is that BAG neurons

341 themselves supply the ILPs that regulate their differentiation. Recently, a number of studies have

342 revealed the functional importance of activity-dependent autocrine signals in circuit development

343 (reviewed in (Herrmann and Broihier 2018)). In mammalian hippocampus, an activity-dependent

344 autocrine Insulin-like Growth Factor 2 (IGF2) signal stabilizes synapses made by dentate

15

345 granule cells onto their postsynaptic partners (Terauchi et al. 2016), and in visual cortex a subset

346 of interneurons generates an activity-dependent autocrine IGF1 signal that regulates the

347 strength of their inhibitory synaptic inputs (Mardinly et al. 2016). Non-insulin like growth factors

348 also function as autocrine signals during nervous system development. Brain-Derived

349 Neurotrophic Factor (BDNF) and Bone Morphogenic Protein (BMP) - like factor homolog have

350 been identified as autocrine signals that regulate synapse development and function in

351 mammalian hippocampus and at the insect neuromuscular junction, respectively (James et al.

352 2014; Harward et al. 2016).

353   Because these autocrine signals are released in an activity-dependent manner, they are

354 able to trigger a mechanism that translates neuronal activity into intracellular signals to regulate

355 gene expression. There are well studied mechanisms that couple neural activity to gene

356 expression via intracellular calcium signaling *e.g.* CREB signaling (West and Greenberg 2011).

357 Gene regulation by autocrine activity-regulated growth factor signals might, however, differ in

358 functionally important ways. An autocrine signal might have a different threshold for activation

359 by neural activity than CREB-dependent mechanisms, allowing for different patterns of neural

360 activity to engage different gene regulatory mechanisms. Once engaged, autocrine signals might

361 act on different timescales, and they likely regulate gene targets distinct from those regulated by

362 CREB. Interestingly, some aspects of BAG neuron development are regulated by CREB (Rojo

363 Romanos et al. 2017). Neural activity, therefore, controls the development of BAG neurons

364 through multiple mechanisms, and these cells will be excellent models for studying the distinct

365 roles in nervous system development of CREB-based excitation-transcription coupling and gene

366 regulation by activity-regulated autocrine signals.

367

Insulin signaling and nervous system development.

During development of *C. elegans* BAG neurons, ILPs inhibit expression of a fully differentiated and functional BAG neuron fate. This role for ILPs differs from their established function as regulators of cell proliferation during nervous system development in both insects and mammals (Fernandez and Torres-Aleman 2012). During development of the *Drosophila* nervous system, ILPs are produced by glial cells in response to nutritive cues, and trigger adjacent neural stem cells to exit quiescence and begin dividing (Chell and Brand 2010; Sousa-Nunes et al. 2011). In mammals insulin-like signaling factors promote neural stem cell proliferation; changing IGF1 levels in the developing rodent brain correspondingly alters brain size (D'Ercole et al. 1996). Mammalian IGF-1 has been shown to function as a mitogenic signal during corticogenesis, and recruits neural progenitors to the cell-cycle (Mairet-Coello et al. 2009). A related factor - IGF2 - promotes the maintenance and expansion of neural stem cells in mammals (Ziegler et al. 2014), and also regulates the proliferation of cerebral cortical progenitors (Lehtinen et al. 2011). We observed a role for ILPs in nervous system development that is distinct from their known function as regulators of proliferation, and found that ILPs repress the differentiation of a specific neuron-type. Both functions of ILPs in nervous system development have in common, however, that they delay the appearance of fully differentiated and functional neurons – either by promoting proliferation of neuronal stem cells at the expense of their differentiation, or by inhibiting expression of specific neuronal cell fates.

C. elegans express a large number of ILPs, many in the nervous system. Insulin-like receptor and its associated signaling factors are also expressed throughout the *C. elegans* nervous system, as is PMK-3, which we show regulates ILP gene expression. It is, therefore, likely that the ILP-dependent mechanism that we have found in developing chemosensory

17

391 neurons, also functions to regulate the differentiation of other neuron-types in *C. elegans*.

392 Furthermore, the molecular constituents of ILP signaling pathways are conserved between

393 nematodes and vertebrates. We suggest, therefore, that autocrine ILP signals might play similar

394 roles in the regulation of neuronal cell fates during development of the vertebrate nervous

395 system.

396

397 **Materials and Methods**

398 *Strains*

399 All strains used in this study were cultivated under standard conditions (Brenner 1974) at 20°C,

400 and are listed in **Supplementary File 1**. The *daf-16(wz151)* deletion strain was generated by

401 CRISPR/Cas9-mediated mutagenesis using Cas9 ribonucleoprotein (Paix 2015), along with a

402 co-CRISPR strategy to increase efficiency (Kim et al. 2014), as previously described (Zamanian

403 et al. 2018). Transgenic animals were generated via microinjection as previously described

404 (Mello 1991).

405

406 *Plasmids*

407 Plasmids used in this study were made using Gibson assembly (Gibson et al. 2009) and are

408 listed in **Supplementary File 2**. The *daf-28(sa191)* cDNA was purchased as a gene block from

409 Integrated DNA Technologies and cloned into the pPD49.26 fire vector using Gibson cloning.

410

411 *Microscopy*

412 Animals were mounted on 2% agarose pads made in M9 medium and immobilized with 30 mM

413 sodium azide (NaN_3). Fluorescence and differential interference contrast (DIC) micrographs

18

414 were acquired with a Zeiss Axioimager M2 upright microscope equipped with an EM-CCD

415 camera (Andor) using a 100x objective (1.4 N.A.). Z-stacks were obtained with an LSM700 laser-

416 scanning confocal microscope (Zeiss) using a 40x objective (1.4 N.A.). Maximum projections of

417 image stacks were generated with Fiji (Schindelin et al. 2012).

418

419 *CO$_2$ avoidance assays*

420 CO_2 avoidance assays were performed as previously described (Brandt and Ringstad 2015).

421 Briefly, a total of 40-50 adult hermaphrodites were confined to a custom-made chamber on an

422 unseeded 10-cm NGM plate fitted with inlets of air and 10% CO_2. Gas mixes were pushed into

423 the chamber at 1.5 mL/min using a syringe pump (New Era, Inc.). After 35 minutes, an avoidance

424 index (A.I.) was computed according to the following equation: $A.I. = \frac{N_{air} - N_{CO_2}}{total\ number\ of\ animals}$.

425

426 *in vivo calcium imaging*

427 *In vivo* calcium imaging was performed as previously described (Smith et al. 2013; Brandt and

428 Ringstad 2015) using the ratiometric calcium indicator YC3.60 (Nagai et al. 2004).

429

430 *Quantification of GRASP puncta*

431 The number and size of GRASP puncta were quantified using Fiji (Schindelin et al. 2012). Z-

432 stacks of the BAG synaptic zone were thresholded and subjected to particle analysis, which

433 automatically drew Region of Interests (ROIs) around puncta whose fluorescence intensity was

434 above background. The number of puncta was defined as the number of particles found in the

435 synaptic zone, and the area of each particle was measured to determine the size of the GRASP

436 puncta. Each particle was manually inspected to confirm that it contained one GRASP puncta;

19

437   if a particle encompassed multiple puncta - separate ROIs were manually drawn around the

438   individual puncta.

439

440   *Genetic suppressor screen for regulators of p38 MAPK-dependent BAG cell development*

441   *pmk-3* mutant animals carrying the BAG fate marker *ynIs64[P_{flp-17}::GFP]* were mutagenized with

442   47 mM ethyl methane sulfate (EMS) as described (Brenner 1974), and screened in the F2

443   generation for restored GFP expression on a Leica M165 FC fluorescence dissecting

444   microscope. Approximately 10% of *pmk-3* mutants express *P_{flp-17}::GFP*, therefore mutants were

445   identified as candidate suppressors of *pmk-3* if more than 50% of their F3 progeny had restored

446   GFP expression.

447

448   *Mapping and cloning of suppressor alleles*

449   Initial round of screening identified two non-complementing alleles, *wz75* and *wz76*. High-

450   resolution-SNP-mapping of *wz75* was performed by crossing *wz75* mutants to the polymorphic

451   strain CB4856 and identifying crossovers using restriction fragment polymorphisms (snip-SNPs)

452   (Davis et al. 2005), which placed *wz75* in a 5 Mbp interval on LG IV. Whole-genome sequencing

453   revealed that *wz75* and *wz76* mutants carry mutations in *unc-31*: *wz75* contains a G → A

454   mutation predicted to change Trp971 to an Amber stop, and *wz76* contains a G → A mutation

455   predicted to disrupt a splice-donor/acceptor site. Further screening and complementation tests

456   identified 3 additional alleles of *unc-31: wz112, wz127*, and *wz130 .* Whole genome sequencing

457   of *wz112* and *wz130* revealed that *wz112* is a G → A missense mutation predicted to change

458   Asp422 to Asn, and *wz130* is a G → A nonsense mutation predicted to change Trp1114 to an

20

459   Opal stop. Sanger sequencing of *wz127* showed that it is a C → T mutation predicted to change

460   Gln15 to an Amber stop.

461

462   *Transgene Expression Analysis*

463   Animals were immobilized as described above. Reporter transgene expression was quantified

464   using the 20x (.8 NA) objective on a Zeiss Axioimager M2 upright microscope equipped with an

465   EM-CCD camera (Andor). To determine the penetrance of transgene expression, we measured

466   the number of BAG cells expressing the reporter in each animal. As an alternative method, we

467   counted the percentage of animals expressing the reporter on a Leica M165 FC fluorescence

468   dissecting microscope. To determine the levels of reporter transgene expression, we measured

469   the mean pixel values in a 30 or 50-pixel-radius circular ROI centered on the BAG soma using

470   Fiji (Schindelin et al. 2012). For all experiments, data was collected over three days.

471

472   *Heat shock experiments*

473   *pmk-3(ok169)* mutant animals carrying a $P_{hsp16.41}$*::irk-1* transgene were shifted twice to 37°C for

474   a half hour, with a one hour recovery at 20°C in between. After heat shock, animals resumed

475   growth at 20°C. Heat-shocked embryos and larvae were assayed for gene expression when they

476   reached adulthood, while adults were assayed 24 hours after heat shock.

477

478   *Cell culture and FACS Sorting for RNA-Seq*

479   Embryonic cell cultures were prepared from wild-type and *pmk-3(wz31)* mutant animals

480   expressing the BAG-specific and *pmk-3* independent marker *wzIs113[P$_{gcy-9}$::GFP]*, as previously

481   described (Christensen 2002; Zhang 2002). In brief, embryos were isolated from synchronized

21

482   populations of hypochlorite treated hermaphrodites, and dissociated into single cells by chitinase

483   treatment. Cells were resuspended in L-15 medium supplemented with 10% FBS (Sigma) and

484   antibiotics, and passed through a 5 μm syringe filter (Millipore). Cells were plated onto poly-D-

485   lysine coated single-well chambered cover glasses (Lab-Tek II) and incubated overnight at 25°C.

486   GFP-labeled BAG neurons were isolated approximately 24 hours after dissociation using

487   Fluorescence Activated Cell Sorting (FACS); sorted cells were confirmed to be >90% GFP

488   positive by direct inspection on a fluorescent microscope. Non-fluorescent, 'non-BAG', cells were

489   also collected. Dead cells were marked with propidium-iodide and excluded from sorted cells.

490   Sorting was performed on a FACSAria Ilu SORP cell sorter using a 70 μm nozzle. Cells were

491   sorted directly into RNA Extraction Buffer (10,000 cells/100 μL buffer), and RNA was purified

492   using the Arcturus PicoPure RNA Isolation Kit (Thermo Fisher). RNA integrity and concentration

493   were evaluated using an Agilent Bioanalyzer. RNA samples had an RNA Integrity score of at

494   least 8, indicating that all samples were of high quality. Two biological replicates were prepared

495   from each cell type.

496

497   *RNA-Seq Analysis of wild type and pmk-3 mutant BAG neurons*

498   cDNA libraries were prepared from RNA (1-2 ng) using the Ovation RNA-Seq System V2

499   (NuGEN), multiplexed, and sequenced as 100 base pair paired end reads using the HiSeq 2500

500   (Illumina). Reads were aligned to the *Caenorhabditis elegans* genome and transcriptome

501   (Wormbase WS243) using the STAR software package (Dobin et al. 2013). Gene expression

502   quantification was performed using HTSeq (Anders 2014). Differential expression analysis was

503   done using the DeSeq2 package (Love et al. 2014) in R. Heatmaps were generated using gplots

504   (Warnes 2016) and RColorBrewer (Neuwirth 2014) R software packages. Read coverage

22

505 histograms were generated from genomic alignments (BAM files) using Integrative Genomics

506 Viewer (Thorvaldsdottir et al. 2013).

507

508 *DAF-16::GFP Localization*

509 Z-stacks were collected from animals expressing $P_{BAG}::daf-16::GFP$ as described above, and

510 image analysis was performed in Fiji (Schindelin et al. 2012). For each cell, the maximum sum

511 projection of 5 stacks (~1 μm/stack) was generated. ROIs were drawn around the nucleus and

512 cell body in a summated projection image, and the total amount of DAF-16::GFP fluorescence

513 was measured in each region. The amount of fluorescence in the cytoplasm was defined as the

514 total amount of DAF-16::GFP fluorescence in the cell body minus the amount in the nucleus. We

515 then computed the ratio of nuclear DAF-16::GFP fluorescence to cytoplasmic DAF-16::GFP

516 fluorescence to monitor insulin activity.

517

518 *Statistical Analysis*

519 Standard error of the mean (SEM) and *P*-values for statistical analyses were calculated using

520 GraphPad Prism Software.

521

522 **Acknowledgments**

528   assisted cell sorting was performed by the Cytometry and Cell Sorting Laboratory at NYU School

529   of Medicine. Whole-genome sequencing and differential gene expression analysis was

530   performed by the NYU School of Medicine Genome Technology Center. Some strains were

531   provided by the CGC, which is funded by the NIH Office of Research Infrastructure Programs

532   grant P40 OD010440, and the Mitani lab (Tokyo Women's Medical University, Japan).

533

534   **Author Contributions**

535   L.B.H. and N.R. designed and performed experiments, interpreted data, and wrote the

536   manuscript. J.P.B. performed genetic suppressor screens and mapping experiments.

537

538   **Competing Interests**

539   The authors declare no competing interests.

540

541   **Figure Legends**
542

543   **Figure 1: PMK-3 mutation affects neuropeptide expression, chemotransduction and**

544   **synapse morphology in chemosensory BAG neurons.**

545   A. Overlaid differential interference contract (DIC) and fluorescence micrographs of wild-type

546   and *pmk-3(wz31)* mutant animals expressing $P_{flp-17}::GFP$, a marker of differentiated BAG cells.

547   B. CO_2-avoidance indices of the wild type, *pmk-3(ok169)*, *flp-17(n4894)*, and *egl-6(n4536)*

548   mutants. N >= 5 independent trials. $P < 0.0001$ for wild type vs. *pmk-3*, and $P = 0.0007$ for

549   wild-type vs. *flp-17*, ordinary one-way ANOVA followed by Tukey's multiple comparisons test.

550   Error bars represent SEM.

551   C. Average calcium responses of wild-type and *pmk-3(ok169)* mutant BAG cells to 10% CO_2

552   stimuli. Shaded area represents the mean $\pm$ SEM. N > 26 animals/genotype. (R/R_0) is the ratio

553   of YFP/CFP emissions normalized to the pre-stimulus ratio.

554   D. Cumulative probability plots of the peak calcium responses (R/R_0) in wild-type and

555   *pmk-3(ok169)* mutant BAG cells to CO_2 stimuli. *P* = 0.0038, unpaired t-test.

556   E. Fluorescence micrographs of BAG GRASP puncta in wild-type and *pmk-3(ok169)* mutant

557   BAG cells using *P*$_{gcy-9}$*::nlg-1::GFP*$_{1-10}$ *P*$_{odr-2b}$*::nlg-1::GFP*$_{11}$, overlaid with *P*$_{gcy-9}$*::dsRed* to label

558   BAG cells.

559   F. Quantification of the size of GRASP puncta in wild-type and *pmk-3(ok169)* mutant BAG cells.

560   N > 28 animals/genotype. *P* = 0.0007, unpaired t-test. Error bars represent SEM.

561
562
563

564   **Figure 2: Mutation of genes required for regulated neuronal secretion suppress the**

565   **defects caused by loss of PMK-3.**

566   A-B. Overlays of DIC and fluorescence micrographs of a *pmk-3(wz31)* mutant (A) and a *pmk-*

567   *3(wz31)* mutant animal carrying the suppressor mutation *wz75* (B) expressing *P*$_{flp-17}$*::GFP*.

568   (Scale bar:10 μm).

569   C. Penetrance of *P*$_{flp-17}$*::GFP* expression in the wild type, *pmk-3(wz31)*, *pmk-3(wz31) sup(wz75)*

570   mutant animals, and in animals carrying a mutation in the suppressor gene on its own,

571   *sup(e169)*.

572   D. Structure of the *unc-31* locus. *wz75, wz76, wz112, wz127* and *wz130* are 5 non-

573   complementing alleles isolated by our *pmk-3* suppressor screen, and *e169* is the *unc-31*

574   reference allele.

575   E. Genes that function with UNC-31/CAPS to regulate secretion of dense core vesicles (DCVs).

576   (VGCC) Voltage-Gated Calcium Channel.

577   F. Penetrance of P_{flp-17}::GFP expression in the wild type, *unc-13(e51)*, *unc-18(e81), unc-*

578   *64(e246)*, *pmk-3*, *unc-13(e51); pmk-3(ok169)*, *pmk-3(ok169); unc-18(e81)*, and *unc-64(e246);*

579   *pmk-3(wz31)* mutants. Data shown for *pmk-3* represent the average penetrance of P_{flp-17}::GFP

580   expression collected from *pmk-3(wz31)* and *pmk-3(ok169)* mutant animals.

581   G. Penetrance of P_{flp-17}::GFP expression in the wild type, *egl-19(n582)*, *unc-2(e55), pmk-*

582   *3(ok169)*, *pmk-3(ok169) egl-19(n582)*, and *pmk-3(ok169); unc-2(e55)* mutants.

583   N > 25 animals/ genotype. (*) $P < 0.05$; (**) $P < 0.01$, (****) $P < 0.0001$, chi-square test.

584
585   **Figure 3: Electrical activity in BAG neurons during development regulates expression of**

586   **a PMK-3-regulated gene.**

587   A. Silencing BAG neural activity using P_{gcy-9}::irk-1 strongly restores the penetrance of P_{flp-17}::GFP

588   expression to *pmk-3(ok169)* mutant BAG cells. Similar effects are observed when pan-neuronal

589   activity is silenced using P_{rab-3}::irk-1.

590   B. BAG-targeted knockdown of *unc-31* using RNAi, P_{gcy-9}::unc-31 RNAi, is sufficient to strongly

591   restore the penetrance of P_{flp-17}::GFP expression to *pmk-3(ok169)* mutant BAG cells, similar to

592   pan-neuronal RNAi of *unc-31*, P_{rab-3}::unc-31 RNAi.

593   N ≥ 25 animals/genotype. (****) $P < 0.0001$, chi-square test.

594   C. Animals carrying a transgene for heat-shock-inducible overexpression of *irk-1*, P_{hsp}::irk-1,

595   were heat-shocked at different developmental stages (embryonic, larval or adult) to induce *irk-1*

596   expression and reduce neural activity.

597   D. Percentage of animals expressing P_{flp-17}::GFP in *pmk-3(ok169)* and *pmk-3(ok169); P_{hsp}::irk-*

598   *1* mutant animals that had been heat shocked at the indicated developmental stages. N > 95

599   animals for all measurements. (****) $P < 0.0001$, ordinary one-way ANOVA followed by Dunnet's

600   multiple comparison test. Bar graph data are plotted as means $\pm$ SEM.

601

602   **Figure 4: PMK-3 represses expression of genes encoding insulin-like peptides in BAG**

603   **chemosensory neurons.**

604   A. Heatmap showing the relative expression of the most differentially expressed genes ($P <$

605   0.001, 129 transcripts) between wild-type (WT) and *pmk-3(wz31)*. Expression of these

606   transcripts in non-BAG cells is also shown. Colors represents standardized Z-scores calculated

607   from the average normalized DeSeq2 read counts, with blue representing low expression and

608   red representing high expression.

609   B. Principal component analysis of the transcriptomes from wild-type BAG cells, *pmk-3(wz31)*

610   mutant BAG cells, and non-BAG cells. Each dot represents one biological replicate.

611   C. Fold-changes of gene expression for insulin like peptides (ILPs) in *pmk-3(wz31)* mutant BAG

612   cells versus wild-type BAG cells. N = 2 biological replicates. (*) $P < 0.05$. (**) $P < 0.01$. (***) $P <$

613   0.001. (****) $P < 0.0001$. P values were adjusted for False Discovery Rates (FDR) using DeSeq2

614   (Love et al. 2014).

615   (D-G). Read coverage histograms for a subset of indicated ILPs that are significantly

616   overexpressed in *pmk-3(wz31)* mutant BAG cells. (see Materials and Methods).

617

618   **Figure 5: Autocrine insulin signaling antagonizes PMK-3-dependent neuropeptide**

619   **expression in BAG neurons.**

620   A. Structure of the *daf-28* locus showing the null allele, *tm2308Δ*, and the dominant negative

621   (dn) *sa191* allele, a point mutation that disrupts production of multiple insulin-like peptides.

27

622   B. Disrupting insulin production in *pmk-3(ok169)* mutant BAG cells by overexpressing

623   *daf-28(sa191)*, P_{BAG}::*daf-28(sa191)*, strongly restores P_{flp-17}::*GFP* expression to *pmk-3(ok169)*

624   mutants. The chromosomal *daf-28(sa191)* mutation also partially restores the percentage of

625   *pmk-3(ok169)* mutants expressing P_{flp-17}::*GFP*. (***) P = 0.0002, (****) P < 0.0001, unpaired t-

626   test.

627   C. *daf-28(tm2308)* partially restores the percentage of *pmk-3(ok169)* mutant animals expressing

628   P_{flp-17}::*GFP*. (****) P < 0.0001, unpaired t-test.

629   D. A canonical insulin signaling pathway conserved between nematodes and vertebrates.

630   E. Percent animals expressing P_{flp-17}::*GFP* in *pmk-3(ok169)*, *daf-2(e1370); pmk-3(ok169)*,

631   *age-1(hx546); pmk-3(ok169)*, *pmk-3(ok169); akt-1(ok525)*, and *pmk-3(ok169); akt-2(ok393)*

632   mutant animals. For the *pmk-3* versus *daf-2; pmk-3* and *pmk-3* versus *age-1; pmk-3*

633   comparisons, P = 0.0016 and P < 0.0001, respectively, unpaired t-test.   For the *pmk-3* versus

634   *pmk-3; akt-1* and *pmk-3* versus *pmk-3; akt-2* comparisons, P < 0.0001 and P = 0.9524,

635   respectively, ordinary one-way ANOVA followed by Dunnet's multiple comparisons test.

636   F. BAG cell-targeted knockdown of *daf-2* using RNAi is sufficient to strongly restore P_{flp-17}::*GFP*

637   expression to *pmk-3(ok169)* mutant BAG cells, even in the absence of *daf-16(wz151)*. (****) P <

638   0.0001. For *pmk-3; P_{BAG}::daf-2 RNAi* versus *daf-16; pmk-3; P_{BAG}::daf-2 RNAi*, P = 0.2612. P –

639   values were calculated with an ordinary one-way ANOVA followed by Tukey's multiple

640   comparisons test.

641   N >= 45 animals/genotype. Bar graph data are plotted as means $\pm$ SEM.

642

643   **Figure 6: *pmk-3* mutant BAG neurons experience increased insulin signaling.**

644   A. Fluorescence micrographs of wild-type and *daf-2(e1370)* mutant animals expressing GFP-

645   tagged DAF-16 in the BAG cell, $P_{BAG}::daf-16::GFP$. (Scale bar: 5 μm). (N) nucleus.

646   B. Cumulative probability plots of the nuclear to cytoplasmic DAF-16::GFP fluorescence ratios

647   in wild-type and *pmk-3(ok169)* mutant BAG cells. N = 36 cells from 27 animals for the wild-type

648   and N = 35 cells from 23 animals for *pmk-3* mutants. *P* = 0.0011, unpaired t-test.

649   C. The nuclear-to-cytoplasmic DAF-16::GFP fluorescence ratio is not significantly different

650   between *daf-2(e1370)* and *daf-2(e1370); pmk-3(ok169)* mutant animals. N = 46 cells from 30

651   animals for *daf-2* mutants and N = 45 cells from 28 animals for *daf-2; pmk-3* mutant animals. *P*

652   = 0.2094, unpaired t-test.

653

654   **Figure 7: Disruption of autocrine insulin signaling restores function to *pmk-3* mutant**

655   **BAG neurons.**

656   A. CO_2-avoidance indices of the wild type, *daf-28(sa191)*, *pmk-3(ok169)*, and *pmk-3(ok169);*

657   *daf-28(sa191)* mutants.

658   B. Reducing insulin secretion in *pmk-3(ok169)* mutant BAG cells by overexpressing

659   *daf-28(sa191)*, $P_{BAG}::daf-28(sa191)$, significantly restored CO_2 avoidance behavior to

660   *pmk-3(ok169)* mutants.

661   C. BAG cell-targeted knockdown of the insulin receptor *daf-2* significantly restores CO_2

662   avoidance behavior to *pmk-3(ok169)* mutant animals.

663   N ≥ 10 trials. *P* values were determined by an unpaired t-test.

664   D. Model for p38 MAPK regulation of BAG neuron development via regulation of an activity-

665   dependent autocrine insulin signal.

666
667

29

668 **Supplementary Files**

669 **Supplementary File 1. *C. elegans* strains used in this study.**

670 A table of the *C. elegans* strains used in this study.

671

672 **Supplementary File 2. Plasmids used in this study.**

673 A table of the plasmids constructed in this study, and a table of the plasmids injected and

674 associated concentration.

675
676
677 **References**

678 Anders SP, P.T.; Huber, W. 2014. HTSeq - A Python framework to work with high-throughput
679   sequencing data. *Bioinformatics* **31**: 166-169. DOI: 10.1101/002824.
680 Barbagallo B, Philbrook A, Touroutine D, Banerjee N, Oliver D, Lambert CM, Francis MM.
681   2017. Excitatory neurons sculpt GABAergic neuronal connectivity in the C. elegans
682   motor circuit. *Development* **144**: 1807-1819. DOI: 10.1242/dev.141911.
683 Brandt JP, Aziz-Zaman S, Juozaityte V, Martinez-Velazquez LA, Petersen JG, Pocock R,
684   Ringstad N. 2012. A single gene target of an ETS-family transcription factor determines
685   neuronal CO2-chemosensitivity. *PLoS One* **7**: e34014. DOI:
686   10.1371/journal.pone.0034014.
687 Brandt Julia P, Ringstad N. 2015. Toll-like Receptor Signaling Promotes Development and
688   Function of Sensory Neurons Required for a C. elegans Pathogen-Avoidance Behavior.
689   *Current Biology*: 1-11. DOI: 10.1016/j.cub.2015.07.037.
690 Brenner S. 1974. The genetics of Caenorhabditis elegans. *Genetics* **77**: 71-94.
691 Chell JM, Brand AH. 2010. Nutrition-responsive glia control exit of neural stem cells from
692   quiescence. *Cell* **143**: 1161-1173. DOI: 10.1016/j.cell.2010.12.007.
693 Christensen ME, A.; Yin, X.; Fox, R.; Morrison, R.; McDonnell, M.; Gleason, C.; Miller III, D.M.;
694   Strange, K. 2002. A primary culture system for functional analysis of *C. elegans*
695   neurons and muscle cells. *Neuron* **33**: 503-514.
696 Cornils A, Gloeck M, Chen Z, Zhang Y, Alcedo J. 2011. Specific insulin-like peptides encode
697   sensory information to regulate distinct developmental processes. *Development* **138**:
698   1183-1193. DOI: 10.1242/dev.060905.
699 D'Ercole AJ, Ye P, Calikoglu AS, Gutierrez-Ospina G. 1996. The role of the insulin-like growth
700   factors in the central nervous system. *Mol Neurobiol* **13**: 227-255. DOI:
701   10.1007/BF02740625.
702 Davis MW, Hammarlund M, Harrach T, Hullett P, Olsen S, Jorgensen EM. 2005. Rapid single
703   nucleotide polymorphism mapping in C. elegans. *BMC Genomics* **6**: 118. DOI:
704   10.1186/1471-2164-6-118.

705 Dobin A, Davis CA, Schlesinger F, Drenkow J, Zaleski C, Jha S, Batut P, Chaisson M,
706   Gingeras TR. 2013. STAR: ultrafast universal RNA-seq aligner. *Bioinformatics* **29**: 15-
707   21. DOI: 10.1093/bioinformatics/bts635.
708 Emtage L, Aziz-Zaman S, Padovan-Merhar O, Horvitz HR, Fang-Yen C, Ringstad N. 2012.
709   IRK-1 potassium channels mediate peptidergic inhibition of Caenorhabditis elegans
710   serotonin neurons via a G(o) signaling pathway. *J Neurosci* **32**: 16285-16295. DOI:
711   10.1523/JNEUROSCI.2667-12.2012.
712 Feinberg EH, Vanhoven MK, Bendesky A, Wang G, Fetter RD, Shen K, Bargmann CI. 2008.
713   GFP Reconstitution Across Synaptic Partners (GRASP) defines cell contacts and
714   synapses in living nervous systems. *Neuron* **57**: 353-363. DOI:
715   10.1016/j.neuron.2007.11.030.
716 Fernandez AM, Torres-Aleman I. 2012. The many faces of insulin-like peptide signalling in the
717   brain. *Nat Rev Neurosci* **13**: 225-239. DOI: 10.1038/nrn3209.
718 Gibson DG, Young L, Chuang RY, Venter JC, Hutchison CA, 3rd, Smith HO. 2009. Enzymatic
719   assembly of DNA molecules up to several hundred kilobases. *Nat Methods* **6**: 343-345.
720   DOI: 10.1038/nmeth.1318.
721 Gramstrup Petersen J, Pocock R. 2013. Neuronal cell fate decisions: O2 and CO2 sensing
722   neurons require egl-13/Sox5. *Worm* **2**: e27284. DOI: 10.4161/worm.27284.
723 Gruner M, Nelson D, Winbush A, Hintz R, Ryu L, Chung SH, Kim K, Gabel CV, van der Linden
724   AM. 2014. Feeding state, insulin and NPR-1 modulate chemoreceptor gene expression
725   via integration of sensory and circuit inputs. *PLoS Genet* **10**: e1004707. DOI:
726   10.1371/journal.pgen.1004707.
727 Guillermin Manon L, Carrillo Mayra A, Hallem Elissa A. 2017. A Single Set of Interneurons
728   Drives Opposite Behaviors in C. elegans. *Current Biology* **27**: 2630-2639.e2636. DOI:
729   10.1016/j.cub.2017.07.023.
730 Guillermin ML, Castelletto ML, Hallem EA. 2011. Differentiation of carbon dioxide-sensing
731   neurons in Caenorhabditis elegans requires the ETS-5 transcription factor. *Genetics*
732   **189**: 1327-1339. DOI: 10.1534/genetics.111.133835.
733 Harward SC, Hedrick NG, Hall CE, Parra-Bueno P, Milner TA, Pan E, Laviv T, Hempstead BL,
734   Yasuda R, McNamara JO. 2016. Autocrine BDNF-TrkB signalling within a single
735   dendritic spine. *Nature* **538**: 99-103. DOI: 10.1038/nature19766.
736 Herrmann KA, Broihier HT. 2018. What neurons tell themselves: autocrine signals play
737   essential roles in neuronal development and function. *Curr Opin Neurobiol* **51**: 70-79.
738   DOI: 10.1016/j.conb.2018.03.002.
739 Hobert O. 2016. Terminal Selectors of Neuronal Identity. *Curr Top Dev Biol* **116**: 455-475. DOI:
740   10.1016/bs.ctdb.2015.12.007.
741 Hobert O, Glenwinkel L, White J. 2016. Revisiting Neuronal Cell Type Classification in
742   Caenorhabditis elegans. *Current Biology* **26**: R1197-R1203. DOI:
743   10.1016/j.cub.2016.10.027.
744 James RE, Hoover KM, Bulgari D, McLaughlin CN, Wilson CG, Wharton KA, Levitan ES,
745   Broihier HT. 2014. Crimpy enables discrimination of presynaptic and postsynaptic pools
746   of a BMP at the Drosophila neuromuscular junction. *Dev Cell* **31**: 586-598. DOI:
747   10.1016/j.devcel.2014.10.006.
748 Kenyon CC, J..; Gensch, E.; Rudner, A.; Tabtiang, R. 1993. A *C. elegans* mutant that lives
749   twice as long as wild type. *Nature* **366**: 461-464.

750 Kim H, Ishidate T, Ghanta KS, Seth M, Conte D, Jr., Shirayama M, Mello CC. 2014. A co-
751   CRISPR strategy for efficient genome editing in Caenorhabditis elegans. *Genetics* **197**:
752   1069-1080. DOI: 10.1534/genetics.114.166389.
753 Kim K, Li C. 2004. Expression and regulation of an FMRFamide-related neuropeptide gene
754   family in Caenorhabditis elegans. *The Journal of comparative neurology* **475**: 540-550.
755   DOI: 10.1002/cne.20189.
756 Kimura KDT, H. A.; Liu, Y.; Ruvkun, F. 1997. *daf-2*, an Insulin Receptor-Like Gene That
757   Regulates Longevity and Diapause in *Caenorhabditis elegans. Science* **277**: 942-946.
758 Lee JS, Shih PY, Schaedel ON, Quintero-Cadena P, Rogers AK, Sternberg PW. 2017.
759   FMRFamide-like peptides expand the behavioral repertoire of a densely connected
760   nervous system. *Proc Natl Acad Sci U S A* **114**: E10726-E10735. DOI:
761   10.1073/pnas.1710374114.
762 Lee RYNH, J.; Ruvkun, G. 2001. Regulation of *C. elegans* DAF-16 and its human ortholog
763   FKHRL1 by the *daf-2* insulin-like signaling pathway. *Current Biology* **11**: 1950-1957.
764 Lee RYNL, L.; Hengartner, M.; Horvitz, H.R.; Avery, L. 1997. Mutations in the alpha1 subunit of
765   an L-type voltage-activated Ca^{2+} channel cause myotonia in *Caenorhabditis elegans*.
766   *The EMBO Journal* **16**: 6066-6076.
767 Lehtinen MK, Zappaterra MW, Chen X, Yang YJ, Hill AD, Lun M, Maynard T, Gonzalez D, Kim
768   S, Ye P et al. 2011. The cerebrospinal fluid provides a proliferative niche for neural
769   progenitor cells. *Neuron* **69**: 893-905. DOI: 10.1016/j.neuron.2011.01.023.
770 Li W, Kennedy SG, Ruvkun G. 2003. daf-28 encodes a C. elegans insulin superfamily member
771   that is regulated by environmental cues and acts in the DAF-2 signaling pathway.
772   *Genes Dev* **17**: 844-858. DOI: 10.1101/gad.1066503.
773 Lin KH, H.; Libina, N.; Kenyon, C. 2001. Regulation of the *Caenorhabditis elegans* longevity
774   protein DAF-16 by insulin/IGF-1 and germline signaling. *Nature Genetics* **28**.
775 Love MI, Huber W, Anders S. 2014. Moderated estimation of fold change and dispersion for
776   RNA-seq data with DESeq2. *Genome Biol* **15**: 550. DOI: 10.1186/s13059-014-0550-8.
777 Mairet-Coello G, Tury A, DiCicco-Bloom E. 2009. Insulin-like growth factor-1 promotes G(1)/S
778   cell cycle progression through bidirectional regulation of cyclins and cyclin-dependent
779   kinase inhibitors via the phosphatidylinositol 3-kinase/Akt pathway in developing rat
780   cerebral cortex. *J Neurosci* **29**: 775-788. DOI: 10.1523/JNEUROSCI.1700-08.2009.
781 Mardinly AR, Spiegel I, Patrizi A, Centofante E, Bazinet JE, Tzeng CP, Mandel-Brehm C,
782   Harmin DA, Adesnik H, Fagiolini M et al. 2016. Sensory experience regulates cortical
783   inhibition by inducing IGF1 in VIP neurons. *Nature* **531**: 371-375. DOI:
784   10.1038/nature17187.
785 Mello CK, J. M.; Stinchcomb, D.; Ambros, V. 1991. Efficient gene transfer in *C. elegans*
786   extrachromosomal maintenance and integration of transforming sequences. *The EMBO*
787   *Journal* **10**: 3959-3970.
788 Morris JZT, H. A.; Ruvkun, G. 1996. A phosphatidylinositol-3-OH kinase family member
789   regulating longevity and diapause in *Caenorhabditis elegans. Nature* **382**: 536-539.
790 Mukhopadhyay S, Lu Y, Shaham S, Sengupta P. 2008. Sensory signaling-dependent
791   remodeling of olfactory cilia architecture in C. elegans. *Dev Cell* **14**: 762-774. DOI:
792   10.1016/j.devcel.2008.03.002.
793 Murphy CT, Hu PJ. 2013. Insulin/insulin-like growth factor signaling in C. elegans. *WormBook*:
794   1-43. DOI: 10.1895/wormbook.1.164.1.

795 Nagai T, Yamada S, Tominaga T, Ichikawa M, Miyawaki A. 2004. Expanded dynamic range of
796   fluorescent indicators for Ca(2+) by circularly permuted yellow fluorescent proteins. *Proc*
797   *Natl Acad Sci U S A* **101**: 10554-10559. DOI: 10.1073/pnas.0400417101.
798 Neuwirth E. 2014. RColorBrewer: ColorBrewer Palettes. R Package, Version 1.1-2.
799 Paix AF, A.; Rasoloson, D.; Seydoux, G. 2015. High efficiency, homology-directed genome
800   editing in *C. elegans* using CRISPR/Cas9 ribonucleoprotein complexes. *Genetics* **208**.
801 Paradis SR, G. 1998. *Caenorhabditis elegans* Akt/PKB transduces insulin receptor-like signals
802   from AGE-1 KI3 kinase to the DAF-16 transcription factor. *Genes and Development* **12**:
803   2488-2498.
804 Peckol EL, Troemel ER, Bargmann CI. 2001. Sensory experience and sensory activity regulate
805   chemosensory receptor gene expression in Caenorhabditis elegans. *Proc Natl Acad Sci*
806   *U S A* **98**: 11032-11038. DOI: 10.1073/pnas.191352498.
807 Peckol ELZ, J.A.; Yarrow, J.C.; Barmann, C.I. 1999. Sensory activity affects sensory axon
808   development in *C. elegans*. *Development* **126**: 1891-1902.
809 Richmond JED, W. S.; Jorgensen, E. M. . 1999. UNC-13 is required for synaptic vesicle fusion
810   in *C. elegans*. *Nature* **2**: 959-964.
811 Ringstad N, Horvitz HR. 2008. FMRFamide neuropeptides and acetylcholine synergistically
812   inhibit egg-laying by C. elegans. *Nature neuroscience* **11**: 1168-1176. DOI:
813   10.1038/nn.2186.
814 Rojo Romanos T, Petersen JG, Pocock R. 2017. Control of Neuropeptide Expression by
815   Parallel Activity-dependent Pathways in Caenorhabditis elegans. *Sci Rep* **7**: 38734.
816   DOI: 10.1038/srep38734.
817 Rojo Romanos T, Petersen JG, Riveiro AR, Pocock R. 2015. A novel role for the zinc-finger
818   transcription factor EGL-46 in the differentiation of gas-sensing neurons in
819   Caenorhabditis elegans. *Genetics* **199**: 157-163. DOI: 10.1534/genetics.114.172049.
820 Sagasti AH, N.; Hyodo, J.; Tanaka, M.; Matsumoto, K.; Bargmann, C.I. 2001. The CamKII
821   UNC-43 activates the MAPKKK NSY-1 to execute a lateral signaling decision required
822   for asymmetric olfactory neuron fates. *Cell* **105**: 221-232.
823 Saifee OW, L.; Nonet, M.L. 1998. The *Caenorhabditis elegans unc-64* locus encodes a
824   syntaxin that interacts genetically with synaptobrevin. *Molecular Biology of the Cell* **9**:
825   1235-1252.
826 Schafer WRK, C.J. 1995. A calcium-channel homologue required for adaptation to dopamine
827   and serotonin in *Caenorhabditis elegans*. *Nature* **375**: 73-78.
828 Schindelin J, Arganda-Carreras I, Frise E, Kaynig V, Longair M, Pietzsch T, Preibisch S,
829   Rueden C, Saalfeld S, Schmid B et al. 2012. Fiji: an open-source platform for biological-
830   image analysis. *Nat Methods* **9**: 676-682. DOI: 10.1038/nmeth.2019.
831 Serrano-Saiz E, Poole RJ, Felton T, Zhang F, De La Cruz ED, Hobert O. 2013. Modular
832   control of glutamatergic neuronal identity in C. elegans by distinct homeodomain
833   proteins. *Cell* **155**: 659-673. DOI: 10.1016/j.cell.2013.09.052.
834 Smith ES, Martinez-Velazquez L, Ringstad N. 2013. A chemoreceptor that detects molecular
835   carbon dioxide. *J Biol Chem* **288**: 37071-37081. DOI: 10.1074/jbc.M113.517367.
836 Sousa-Nunes R, Yee LL, Gould AP. 2011. Fat cells reactivate quiescent neuroblasts via TOR
837   and glial insulin relays in Drosophila. *Nature* **471**: 508-512. DOI: 10.1038/nature09867.
838 Speese S, Petrie M, Schuske K, Ailion M, Ann K, Iwasaki K, Jorgensen EM, Martin TF. 2007.
839   UNC-31 (CAPS) is required for dense-core vesicle but not synaptic vesicle exocytosis in

840   Caenorhabditis elegans. *J Neurosci* **27**: 6150-6162. DOI: 10.1523/JNEUROSCI.1466-
841   07.2007.
842 Sulston JEH, H.R. 1977. Post-embryonic Cell Lineage of the Nematode, *Caenorhabditis*
843   *elegans*. *Developmental Biology* **56**: 110-156.
844 Sulston JES, E.; White, J.G.; Thomson, J.N. 1983. The embryonic cell lineage of the nematode
845   *Caenorhabditis elegans*. *Developmental Biology* **100**: 64-119.
846 Terauchi A, Johnson-Venkatesh EM, Bullock B, Lehtinen MK, Umemori H. 2016. Retrograde
847   fibroblast growth factor 22 (FGF22) signaling regulates insulin-like growth factor 2
848   (IGF2) expression for activity-dependent synapse stabilization in the mammalian brain.
849   *Elife* **5**. DOI: 10.7554/eLife.12151.
850 Thomas GM, Huganir RL. 2004. MAPK cascade signalling and synaptic plasticity. *Nat Rev*
851   *Neurosci* **5**: 173-183. DOI: 10.1038/nrn1346.
852 Thorvaldsdottir H, Robinson JT, Mesirov JP. 2013. Integrative Genomics Viewer (IGV): high-
853   performance genomics data visualization and exploration. *Brief Bioinform* **14**: 178-192.
854   DOI: 10.1093/bib/bbs017.
855 Troemel ERS, A.; Bargmann, C.I. 1999. Lateral signaling mediated by axon contact and
856   calcium entry regulates asymmetric odorant receptor expression in *C. elegans*. *Cell* **99**:
857   387-398.
858 Tullet JM, Hertweck M, An JH, Baker J, Hwang JY, Liu S, Oliveira RP, Baumeister R,
859   Blackwell TK. 2008. Direct inhibition of the longevity-promoting factor SKN-1 by insulin-
860   like signaling in C. elegans. *Cell* **132**: 1025-1038. DOI: 10.1016/j.cell.2008.01.030.
861 Wamsley B, Fishell G. 2017. Genetic and activity-dependent mechanisms underlying
862   interneuron diversity. *Nat Rev Neurosci* **18**: 299-309. DOI: 10.1038/nrn.2017.30.
863 Warnes GRB, B.; Bonebakker, L.; Gentleman, R.; Liaw, W.H.A.; Lumley, T.; Maechler, M.;
864   Magnusson, A.; Moeller, S.; Schwartz, M.; Venables, B. 2016. gplots: Various R
865   Programming Tools for Plotting Data, Version 2.14.1.
866 Weimer RM, Richmond JE, Davis WS, Hadwiger G, Nonet ML, Jorgensen EM. 2003. Defects
867   in synaptic vesicle docking in unc-18 mutants. *Nat Neurosci* **6**: 1023-1030. DOI:
868   10.1038/nn1118.
869 West AE, Greenberg ME. 2011. Neuronal activity-regulated gene transcription in synapse
870   development and cognitive function. *Cold Spring Harb Perspect Biol* **3**. DOI:
871   10.1101/cshperspect.a005744.
872 White JG, Southgate E, Thomson JN, Brenner S. 1986. The structure of the nervous system of
873   the nematode Caenorhabditis elegans. *Philos Trans R Soc Lond B Biol Sci* **314**: 1-340.
874 Zamanian M, Cook DE, Zdraljevic S, Brady SC, Lee D, Lee J, Andersen EC. 2018. Discovery
875   of genomic intervals that underlie nematode responses to benzimidazoles. *PLoS Negl*
876   *Trop Dis* **12**: e0006368. DOI: 10.1371/journal.pntd.0006368.
877 Zhang YM, C.; Delohery, T.; Nasipak, B.; Foat, B.C.; Bounoutas, A.; Bussemak, H.J.; Kim,
878   S.K.; Chalfie, M. 2002. Identification of genes expressed in *C. elegans* touch receptor
879   neurons. *Nature* **418**: 331-335.
880 Zhou KM, Dong YM, Ge Q, Zhu D, Zhou W, Lin XG, Liang T, Wu ZX, Xu T. 2007. PKA
881   activation bypasses the requirement for UNC-31 in the docking of dense core vesicles
882   from C. elegans neurons. *Neuron* **56**: 657-669. DOI: 10.1016/j.neuron.2007.09.015.
883 Ziegler AN, Chidambaram S, Forbes BE, Wood TL, Levison SW. 2014. Insulin-like growth
884   factor-II (IGF-II) and IGF-II analogs with enhanced insulin receptor-a binding affinity

885   promote neural stem cell expansion. *J Biol Chem* **289**: 4626-4633. DOI:
886   10.1074/jbc.M113.537597.
887 Zimmer M, Gray JM, Pokala N, Chang AJ, Karow DS, Marletta MA, Hudson ML, Morton DB,
888   Chronis N, Bargmann CI. 2009. Neurons detect increases and decreases in oxygen
889   levels using distinct guanylate cyclases. *Neuron* **61**: 865-879. DOI:
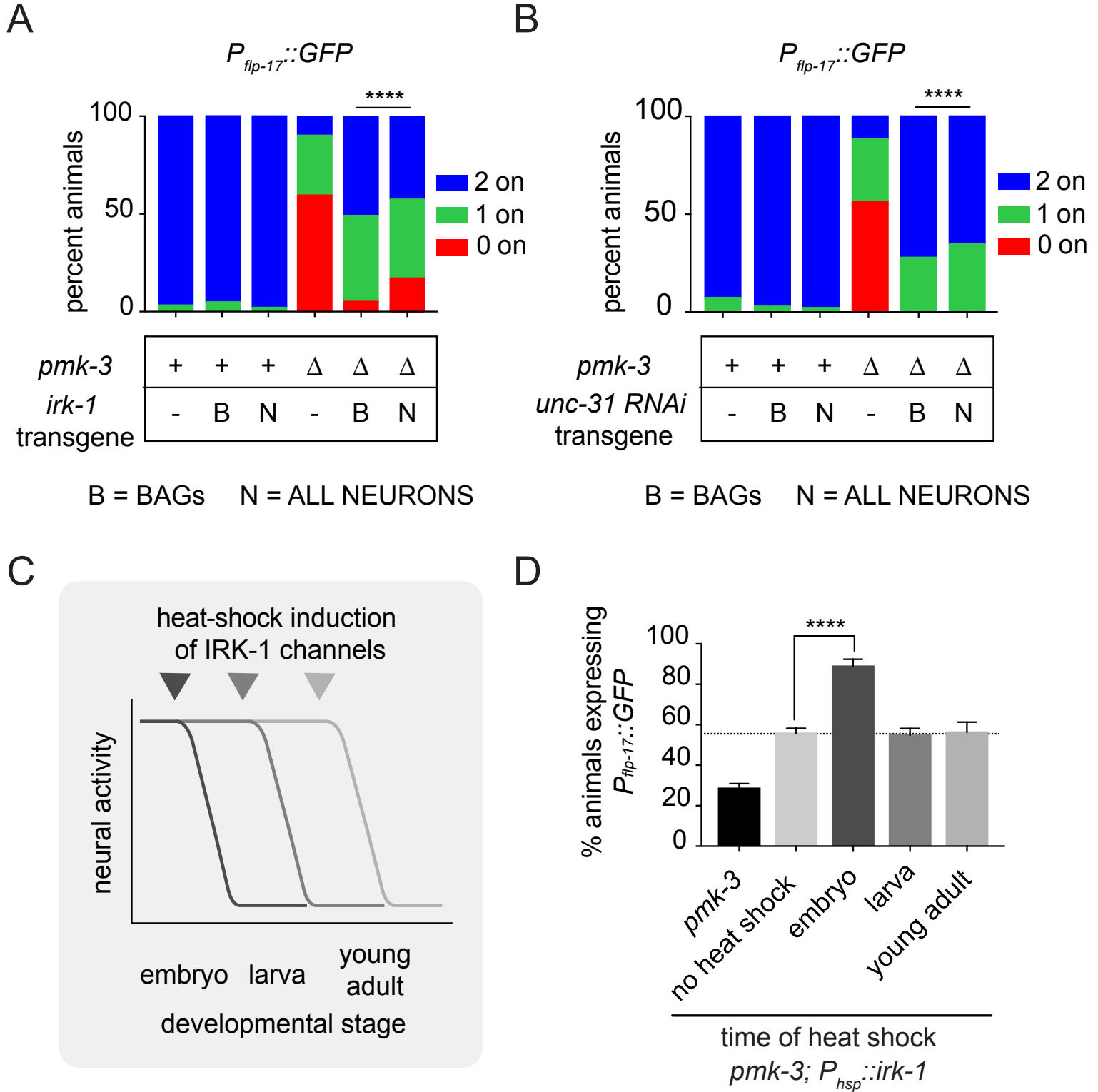890   10.1016/j.neuron.2009.02.013.

891
892
893
894
895
896
897
898
899
900
901
902
903
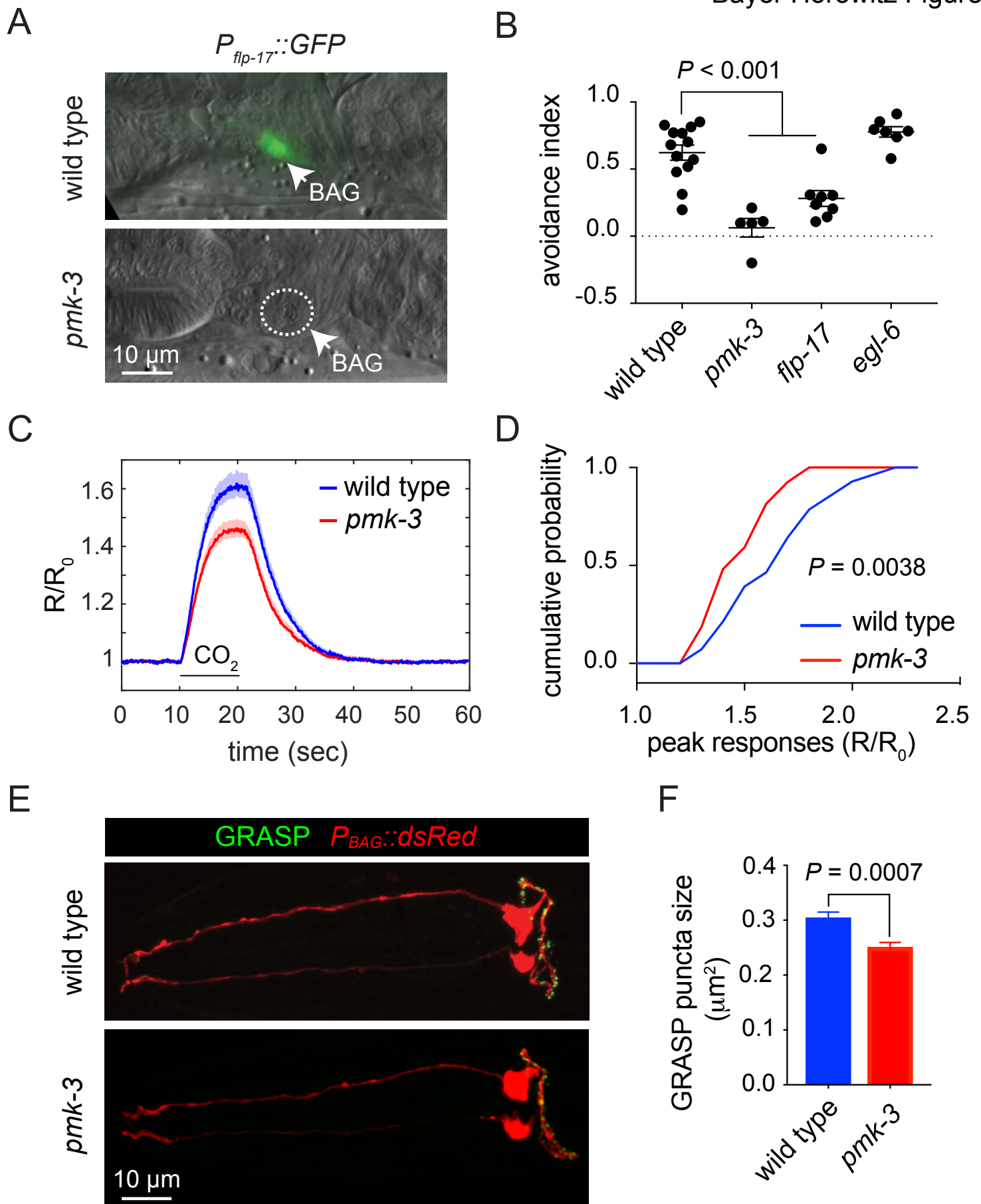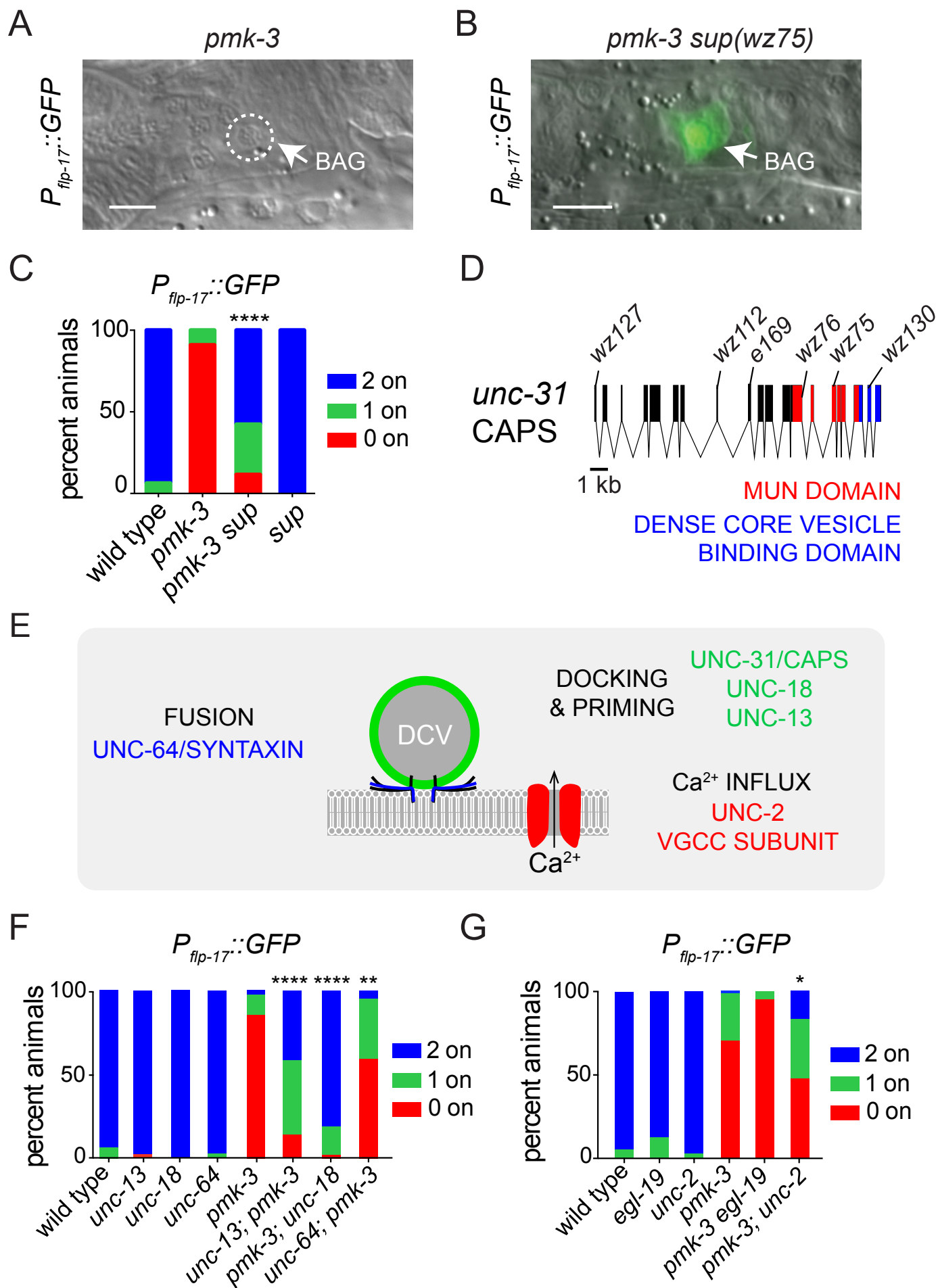
Bayer Horowitz Figure 3

Bayer Horowitz Figure 4

Bayer Horowitz Figure 6
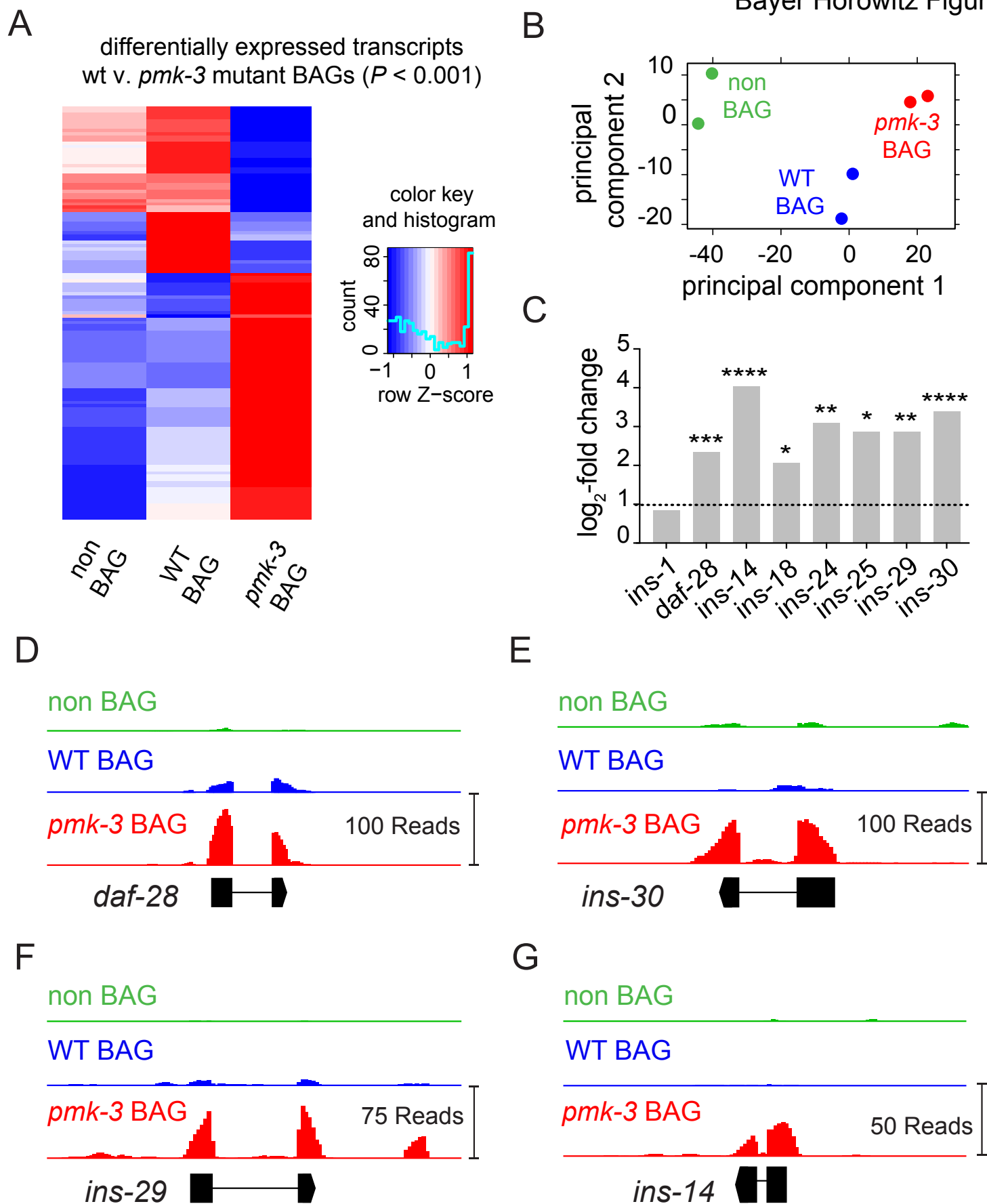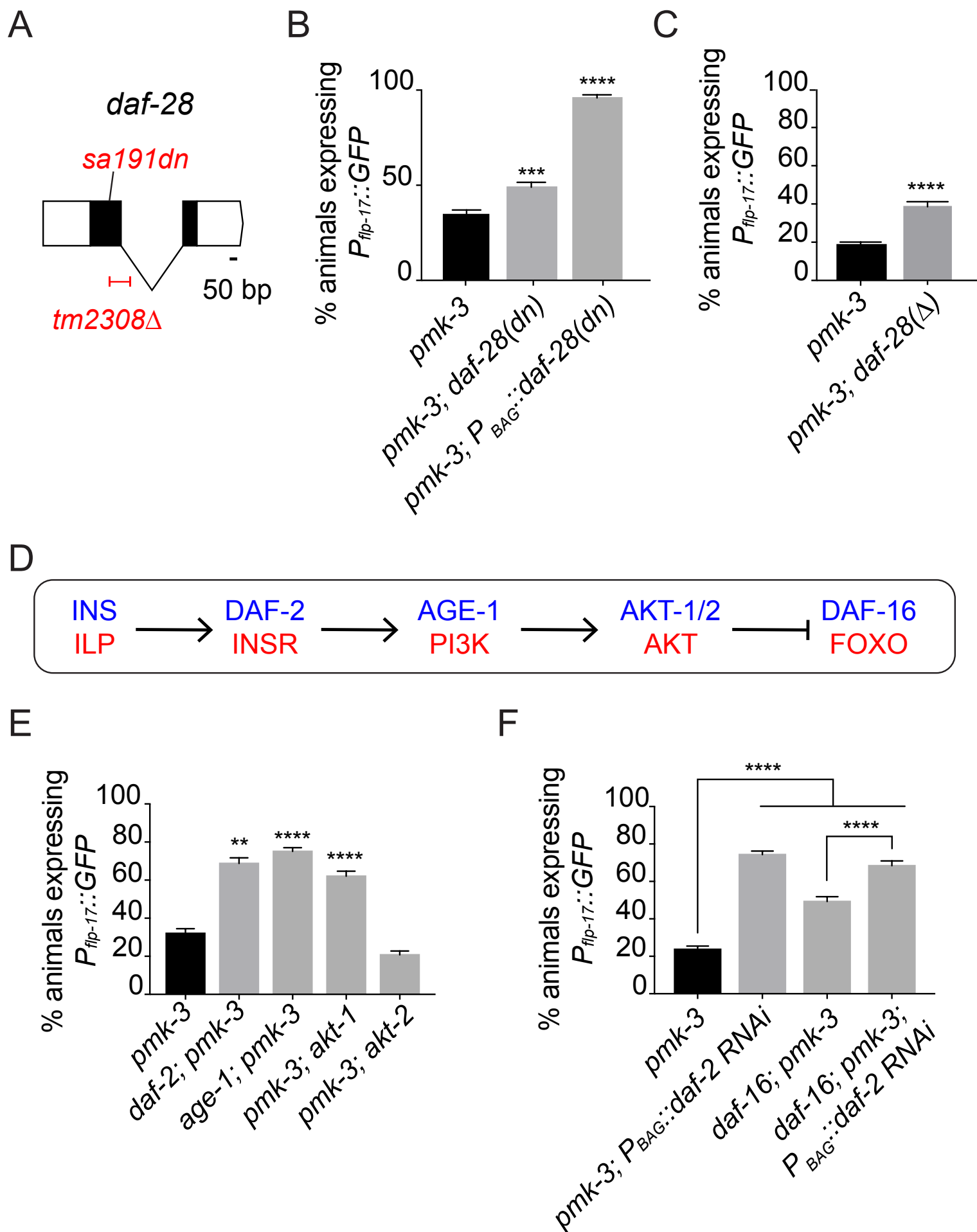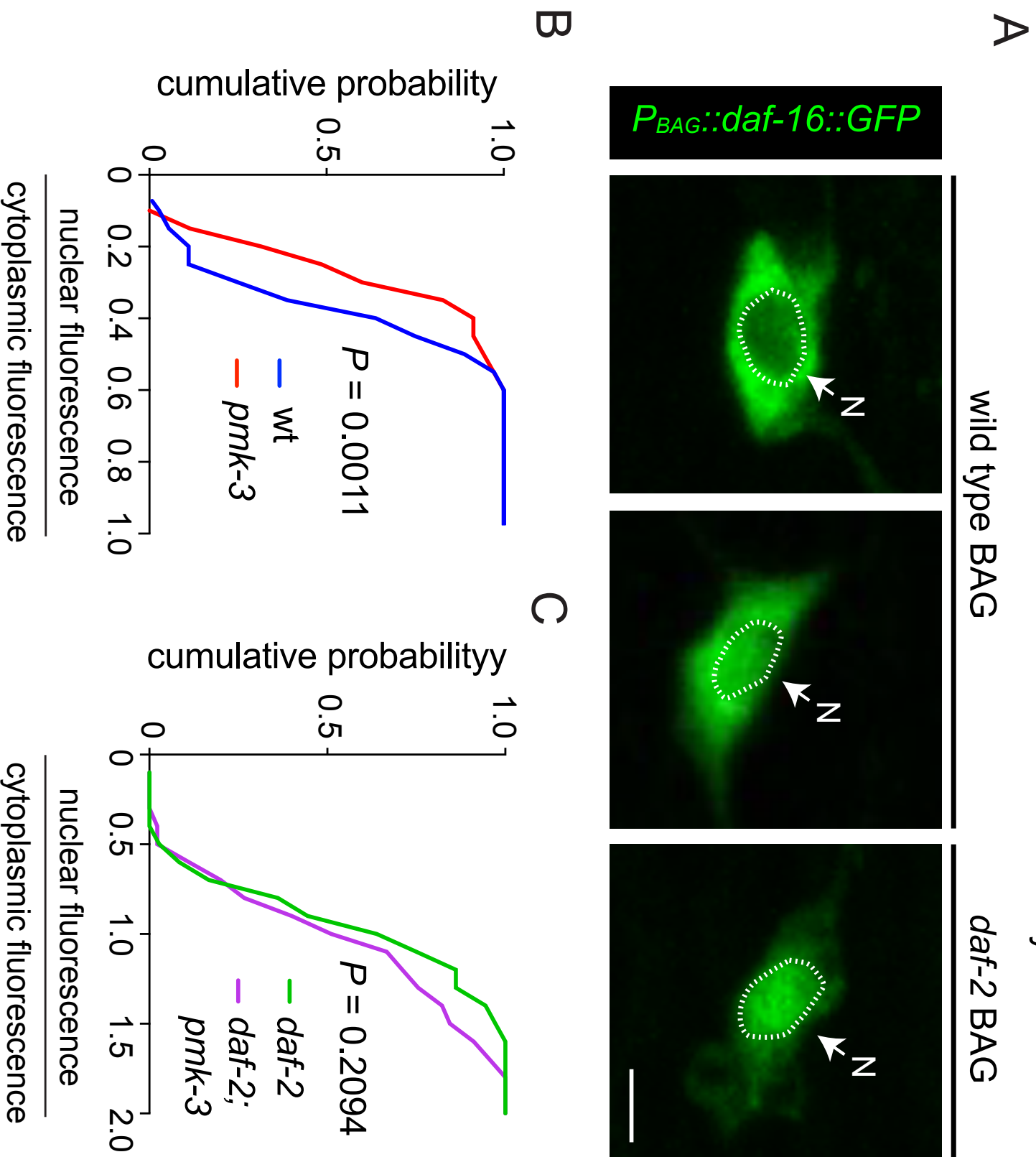
Bayer Horowitz Figure 7

Supplemental Figure S1: *pmk-3* mutant BAG neurons exhibit impaired chemotransduction in CO_2-Sensing BAG neurons
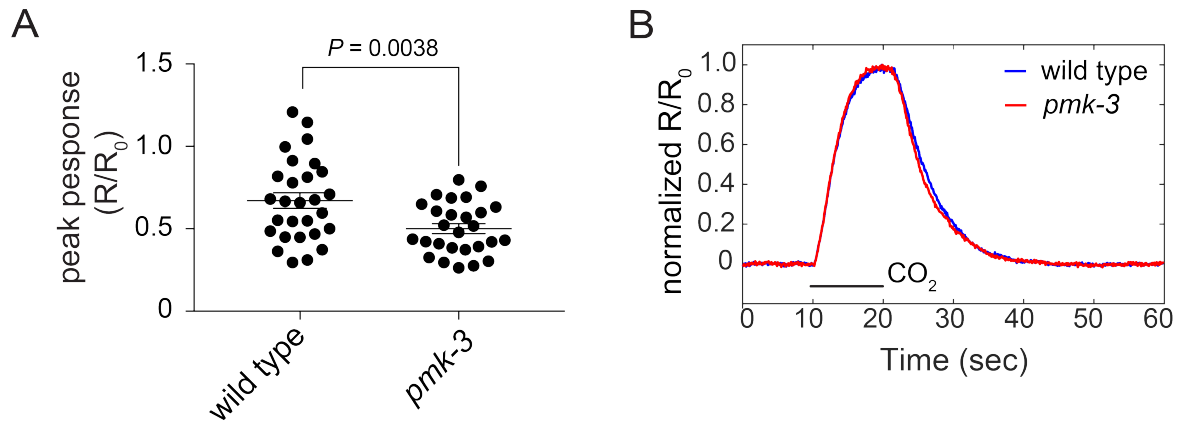
A. Scatter plots showing the distribution of peak calcium responses (R/R_0 values) of wild-type and *pmk-3(ok169)* mutant BAG neurons to 10% CO_2 stimuli. *P* = 0.0038, unpaired t-test. N > 26 animals/genotype. Error bars represent SEM.

B. Dynamics of average calcium responses of wild-type and *pmk-3(ok169)* mutant BAG neurons to 10% CO_2 stimuli.

Supplemental Figure S2: *pmk-3* mutant BAG neurons form normal number of synapses.
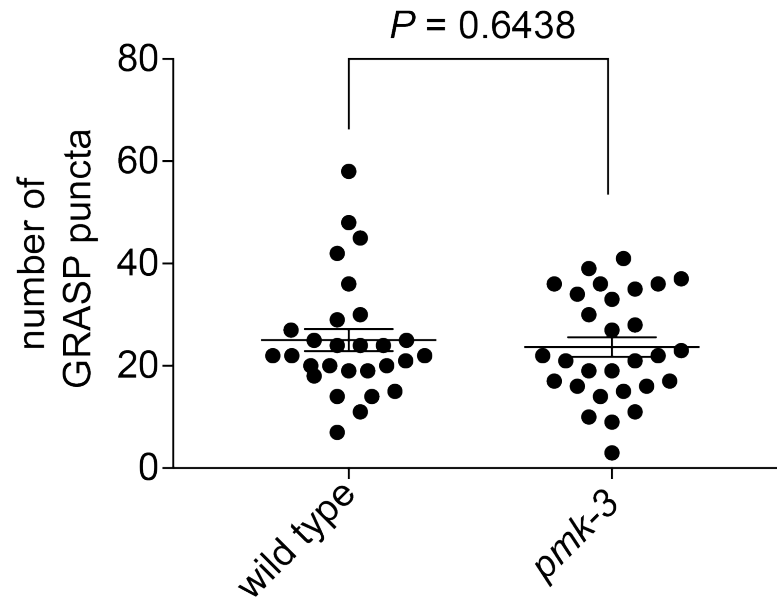
Scatter plot showing the number of GRASP-puncta in wild-type and *pmk-3(ok169)* mutant BAG neurons. *P* = 0.6438, unpaired t-test. N > 28 animals/genotype. Error bars represent SEM.

$P_{flp-17}::GFP$

Supplemental Figure S3: Suppressor mutations partially restore the levels of *flp-17* reporter expression to *pmk-3* mutant BAG cells.
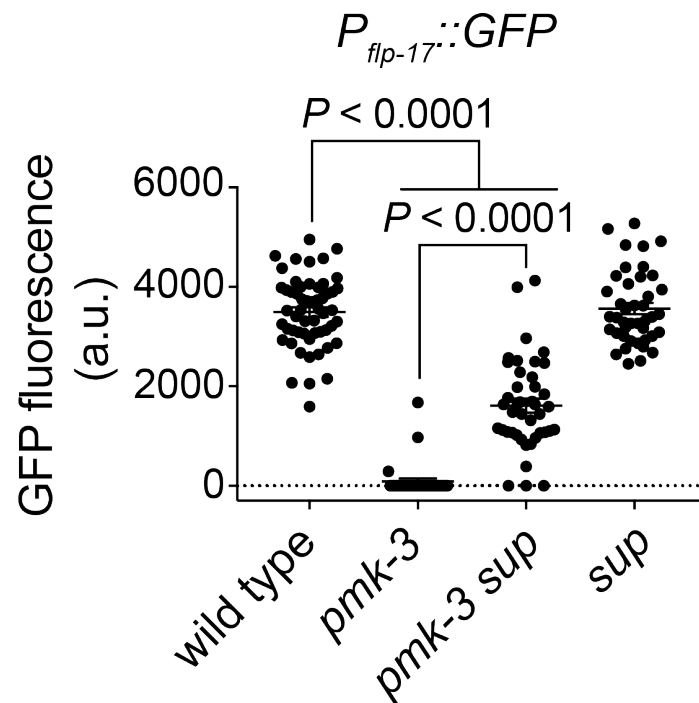
Levels of $P_{flp-17}::GFP$ expression in the wild-type, *pmk-3(wz31)*, *pmk-3(wz31) sup(wz75)*, and *sup(e169)* mutant animals (****) $P < 0.0001$, ordinary one-way ANOVA followed by Tukey's multiple comparison test. N > 20 animals/genotype. (a.u.) arbitrary units. Error bars represent SEM.
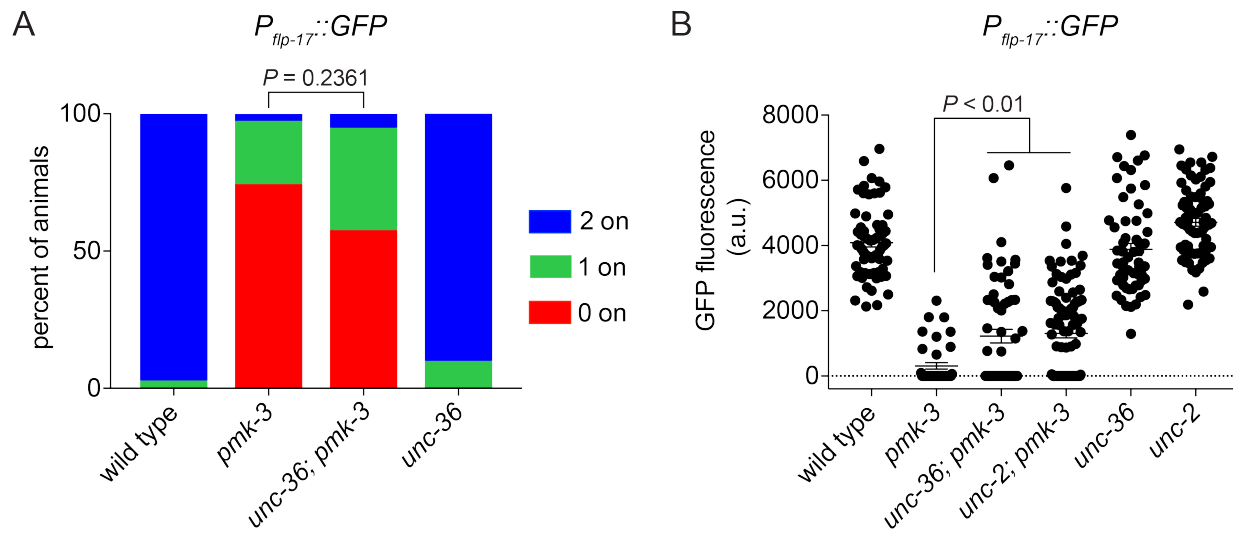
Supplemental Figure S4: Suppressor regulates some, but not all, PMK-3 regulated genes in BAG neurons.
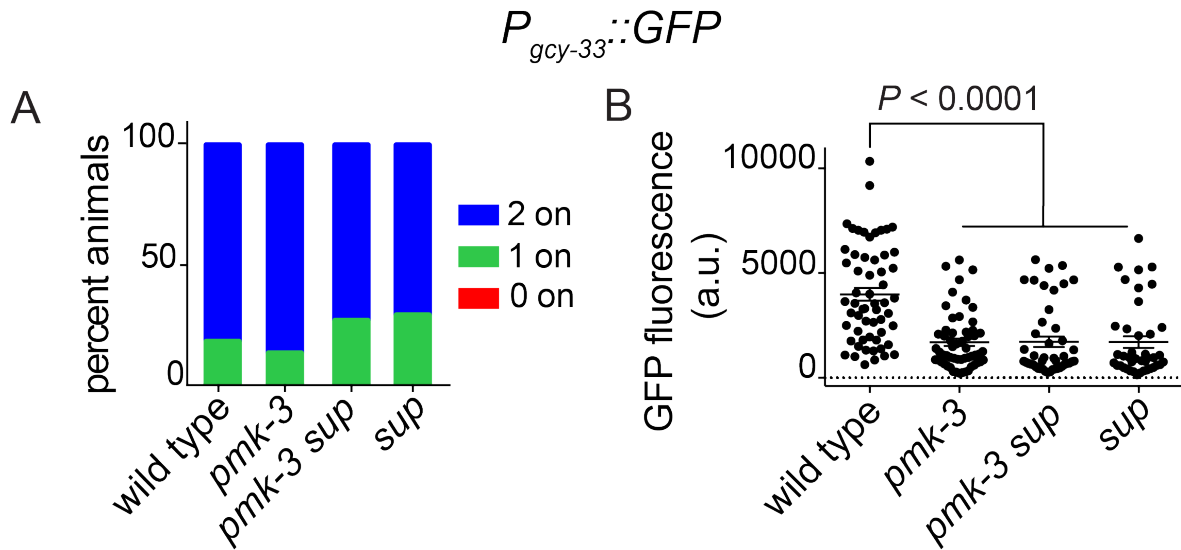
(A). Frequency of $P_{gcy-33}::GFP$ expression in the wild-type, *pmk-3(wz31)*, *pmk-3(wz31) sup(wz75)*, and *sup(e169)* mutant animals.

(B). Levels of $P_{gcy-33}::GFP$ expression in the wild-type, *pmk-3(wz31)*, *pmk-3(wz31) sup(wz75)*, and *sup(e169)* mutant animals. (****) $P < 0.0001$, ordinary one-way ANOVA followed by Tukey's multiple comparison test. N > 20 animals/genotype. (a.u.) arbitrary units. Error bars represent SEM.
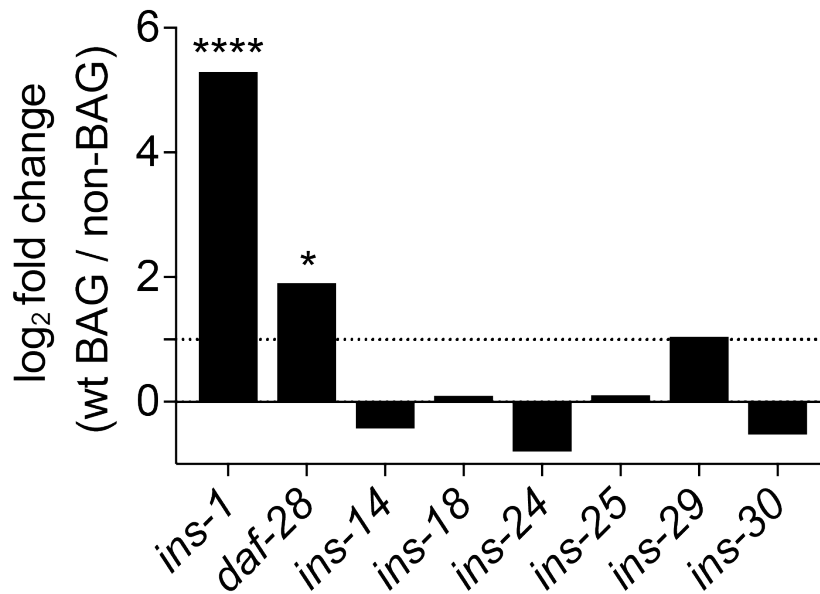
Supplemental Figure S5: Mutations in NPQ-type Voltage Gated Calcium Channel subunits restore *flp-17* expression to *pmk-3* mutant BAG neurons

(A). Penetrance of $P_{flp-17}::GFP$ expression in the wild-type, *pmk-3(ok169)*, *unc-36(e251); pmk-3(ok169)*, and *unc-36(e251)* mutant animals. *P* = 0.2361, chi-square test. N ≥ 30 animals/genotype.

(B). Levels of $P_{flp-17}::GFP$ expression in the wild-type, *pmk-3(ok169)*, *unc-36(e251); pmk-3(ok169)*, *pmk-3(ok169); unc-2(e55)*, *unc-36(e251)*, and *unc-2(e55)* mutant animals. *P* = 0.0028 for *pmk-3* vs *unc-36; pmk-3* and *P* = 0.0003 for *pmk-3* vs *pmk-3; unc-2*, ordinary one-way ANOVA followed by Tukey's multiple comparison test. N ≥ 30 animals/genotype. (a.u.) arbitrary units. Error bars represent SEM.
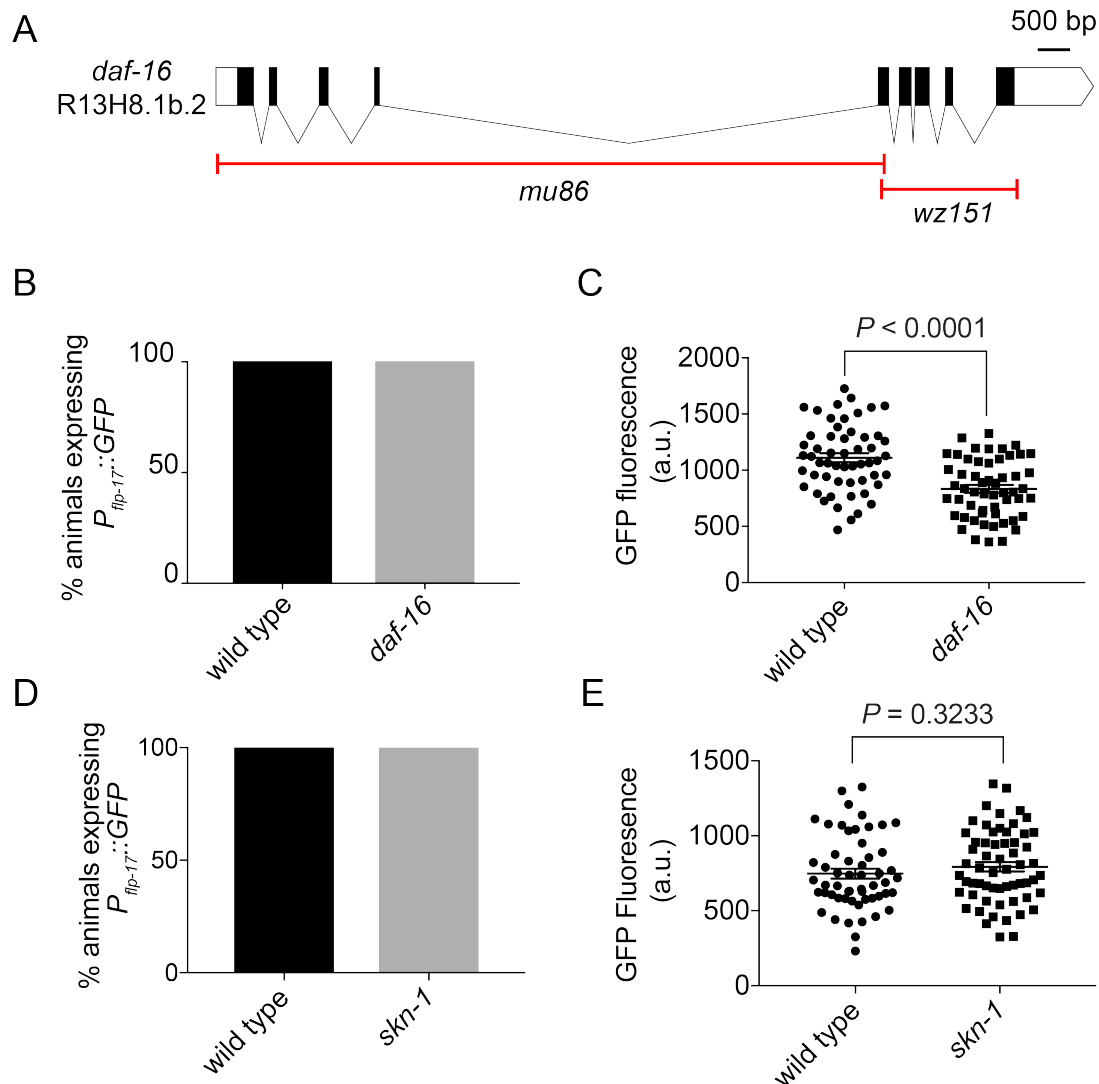
Supplemental Figure S6: The insulin like peptides, *ins-1* and *daf-28*, are enriched in wild-type BAG cells.

Fold changes of gene expression in wild type BAG cells versus non-BAG cells for *ins*-1 and ILPs that are enriched in *pmk-3* mutant BAG cells. (*) $P < 0.05$, (****) $P < 0.0001$.

Supplemental Figure S7: Loss of DAF-16 reduces levels of *flp-17* expression.

(A). Structure of the *daf-16* genetic locus showing the canonical null allele, *mu86*, and the *wz151* 2065 base pair deletion allele generated using CRISPR/Cas9 mutagenesis.

(B). Percentage of wild-type and *daf-16(wz151)* mutant animals expressing $P_{flp-17}::GFP$.

(C). Levels of $P_{flp-17}::GFP$ fluorescence in the wild-type and *daf-16(wz151)* mutant animals. $P < 0.0001$, unpaired t-test.

(D). Percentage of wild-type and *skn-1(zu67)* mutant animals expressing $P_{flp-17}::GFP$.

Because *skn-1(zu67)* is maternal effect lethal, *skn-1(zu67)* homozygous mutants were picked from heterozygous mothers carrying the *mIs11[myo-2::GFP]* balancer chromosome for analysis.

(E). Levels of $P_{flp-17}::GFP$ fluorescence in the wild-type and *skn-1(zu67)* mutant animals.

P = 0.3233, unpaired t-test.

(a.u.) arbitrary units. N > 25 animals/genotype. Error bars represent SEM.